Working Fluid Selection for Organic Rankine Cycle Power Generation Using Hot Produced Supercritical CO_2 from a Geothermal Reservoir

Xingchao Wang [a,*], Edward K. Levy [a], Chunjian Pan[a], Carlos E. Romero [a], Carlos Rubio-Maya [b], Lehua Pan [c]

[a] *Energy Research Center, Lehigh University, 117 ATLSS Dr., Bethlehem, PA 18015, USA*

[b] *Faculty of Mechanical Engineering, Universidad Michoacán de San Nicolas de Hidalgo, Morelia, Michoacán C.P. 58030, Mexico*

[c] *Earth Sciences Division, Lawrence Berkeley National Laboratory, University of California, Berkeley, CA 94720, USA*

Keywords: *Organic Rankine Cycle, Working Fluid Selection, Supercritical CO_2, Geothermal Heat Mining, Power Generation*

Abstract

Geothermal heat mining simulations using T2Well/ECO2N software are performed in this paper. The working fluid selection criteria for ORC power generation using sCO_2 from geothermal reservoirs are presented for subcritical, superheated and supercritical ORC power generation approaches. Meanwhile, the method of working fluid classification for ORC is proposed. In order to get the feasible ORC design, this study introduces the concept of turning point for isentropic and dry working fluids, also minimum turbine inlet temperature for wet working fluids. A thermodynamic model is developed with the capabilities to obtain optimum working fluid mass flow rate and evaluate thermal performance of the three ORC approaches. With this model, thirty potential working fluids with the critical temperatures in the range of 50 ℃ to 225 ℃ are screened considering physical properties, environmental and safety impacts, and thermodynamic performances. Finally, the thermodynamic results are compared in this paper for all possible working fluids and analyses regarding on optimization options are also discussed.

* Corresponding Author. Tel.: +1(610)758-6282; Fax: + 1(610)758-5959.
Email address: xiw611@Lehigh.edu

Nomenclature

Roman symbols

L_0	Geothermal reservoir length [m]
L_1	Injection and production well distance [m]
H_0	Distance from surface of the ground to bottom of the reservoir [m]
H_1	Distance from ground surface to cap rock [m]
H_2	Distance from cap rock to bottom of reservoir [m]
Z	Vertical distance below the ground surface [m]
R	Radial distance from injection well to production well [m]
m_{VG}	Van Genuchten parameter
Q	Heat duty [MW_{th}]
T	Temperature [℃]
p	Pressure [MPa]
h	Specific enthalpy [kJ/kg]
s	Specific entropy [$kJ/kg \cdot K$]
e	Specific exergy [kJ/kg]
$\dot{m}$	Mass flow rate [kg/s]
W_{net}	Net power output [MW_e]
w_{net}	Specific power output [$kW_e/(kg/s)$]
ΔT	Temperature difference [℃]
i	Mesh point
g	Gravitational acceleration [m/s^2]
V	Velocity [m/s]

Subscripts

evp	Evaporator	*scrit*	Supercritical
p	Pump	*s*	Isentropic process
t	Turbine	*cal*	Calculated value
cond	Condenser	*real*	Real value
cr	Critical point	*opt*	Optimum
WF	Working Fluid	0	Reference state
tn	Turning point	min	Minimum
sv	Saturated vapor	*in*	Inlet
th	Thermal	*out*	Outlet
pinch	Pinch point	*error*	Error [%]

Greek letters

υ	Specific Volume [m^3/kg]
ξ	Slope of saturated vapor curve
η	Efficiency [%]
ε	Working fluid type classification factor
σ	Molecular complexity

Acronyms

GWP	Global warming potential
ODP	Ozone depletion potential
sCO_2	Supercritical carbon dioxide
ORC	Organic Rankine cycle
CPG	CO_2-plume geothermal

1. Introduction

Carbon dioxide (CO_2) capture and sequestration in deep saline aquifers technologies have been studied recently as an efficient and feasible way to control the greenhouse gas emissions [1]. A concept injecting CO_2 into geologic reservoirs as a working fluid to recover heat and generate power above the ground has been investigated widely. Using supercritical CO_2 (sCO_2) to replace water to extract heat in the CO_2 based enhanced geothermal system (CO_2-EGS) was firstly proposed by Brown [2]. Pruess et al. extended this concept and conducted numerical simulations to prove the better heat extraction performance and benefits for CO_2 as compared to water in the CO_2-EGS [3, 4]. Recently, studies on high-permeability hydrothermal geothermal reservoirs were conducted by Randolph, Adams and Saar et al.. A concept of CO_2-Plume Geothermal (CPG) systems involving CO_2 injection and production was developed and sCO_2 has been proven to work more efficiently for power generation than water/brine geothermal systems due to its high mobility and substantially density change with temperature resulting a buoyance-driven loop to reduce or eliminate recompression work of CO_2 to reinject back to geothermal reservoirs [5-8]. All these investigations and studies indicate CO_2 can achieve better thermodynamic and economic performance compared to geothermal hot water in power generation applications. In addition, part of injecting CO_2 will be trapped in the geothermal reservoir which is another benefit of this novel application.

The research version of T2Well/ECO2N simulator was used to carry out simulation to obtain the hot produced sCO_2 conditions, such as temperature, pressure and mass flow rate for ORC working fluid selection in this study [9, 10]. The simulation was conducted with the typical reservoir properties and characteristics in Mexico which has been investigated by the authors of this paper recently [11]. This study reports the feasibility of using CO_2 for heat extraction for twenty-one sites in Mexico and presents the totality of fully characterized geothermal sites in Mexico.

Using organic Rankin cycle (ORC) to convert low grade heat source, such as geothermal energy, solar energy, waste heat and biomass energy to electric power has received a lot of attentions recently [12]. As geothermal energy is classified as low-grade heat source, ORC potentially has the capability to generate electricity using hot produced sCO_2 from geothermal reservoirs. The

performance of ORC significantly depends on the working fluid. Hence, the working fluid selection is also very critical to different heat sources. It is still challenging to establish a universal ORC working fluid selection criteria since it is a combined effect of thermal performance, cost and environmental impact with different heat sources conditions [13]. Researches on working fluid selection have been carried out for geothermal hot water, waste heat or solar thermal energy [14-18]. However, the studies on working fluid selection for the ORC power generation using hot sCO_2 are very limited.

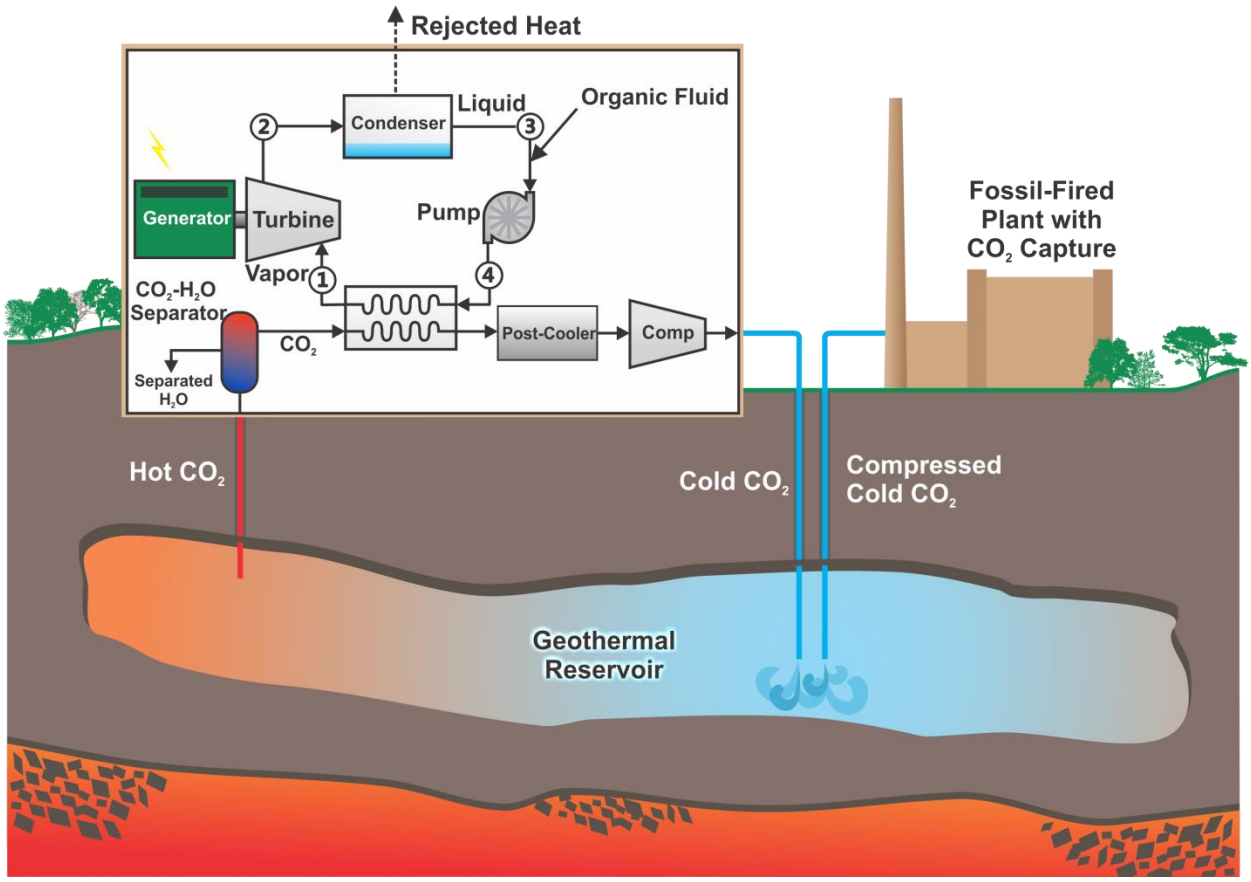

Fig. 1. Sketch of ORC Power Generation Using Hot Produced CO_2 from a Geothermal Reservoir.

In this paper, thirty potential working fluids were screened and selected based on their thermodynamic performances and environmental impacts. The working fluid selection criteria was proposed for the three different types of ORC power generation systems using sCO_2 produced from a geothermal reservoir (Fig. 1). For the obtained heat source conditions: sCO_2 flow rate, pressure and temperature, the optimum working fluid mass flow rate for each possible

working fluid was determined with achieving the pinch temperature (minimum approach in HTX) in the intermediate heat exchanger. Finally, the selected working fluids thermodynamic performances were calculated.

2. Geothermal Reservoir and Wellbore Modeling

2.1 Model Description

A fully coupled geothermal wellbore-reservoir system using CO_2 as the working fluid to extract heat was modeled by Pan et al. who is also the author of this paper [19]. Similarly in this study, the five-spot well pattern is chosen and ¼ molding symmetric domain is used to carry out the simulation (Fig. 2). The geometries of wellbores and reservoir are presented in Fig. 2, Fig. 3 and Table 1. The ¼ of injection well and reservoir with one full production well are assumed in the model domain. To eliminate the effect of reservoir boundaries (zero heat and mass flux), a 4000 m length reservoir was considered in this paper which is different from the previous studies considering a relatively small box reservoir model.

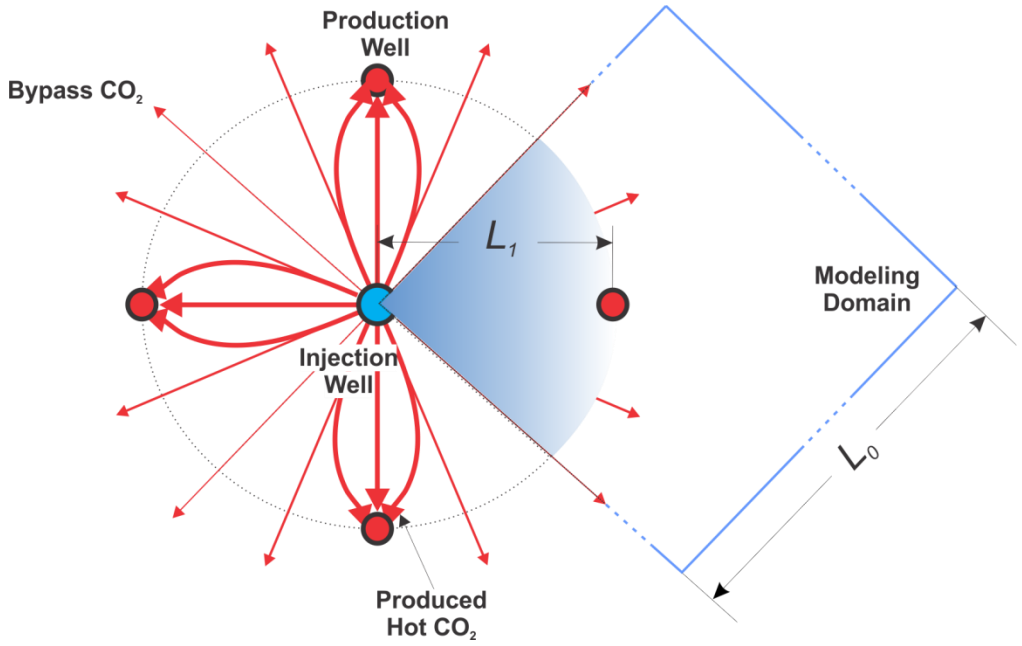

Fig. 2. Five-spot Geothermal Well Pattern and CO_2 Stream Lines in Geothermal Reservoir with ¼ T2Well/ECO2N Modeling Domain.

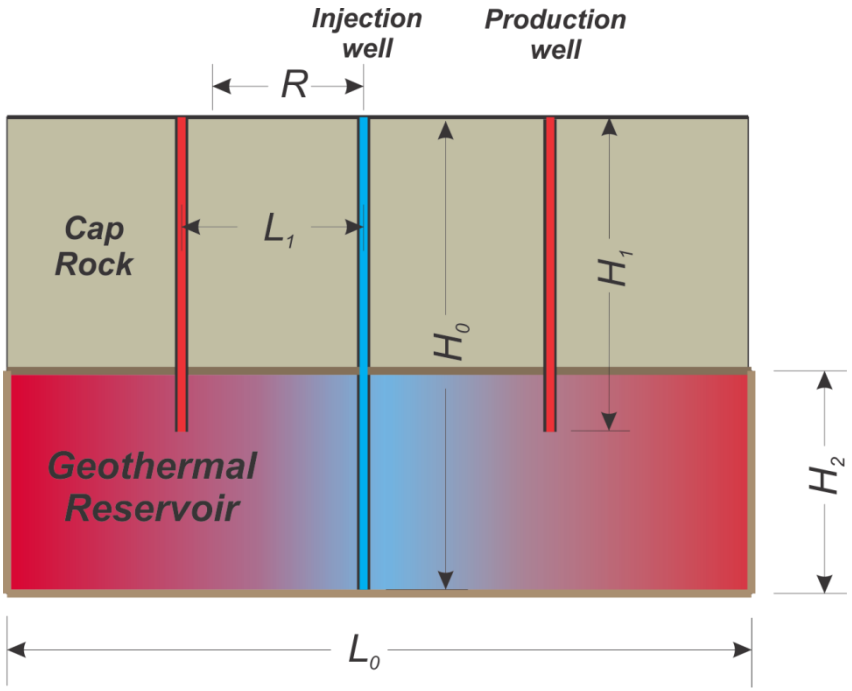

Fig. 3. Geometries Used in the Geothermal Heat Mining Modeling.

Table 1

Reservoir and Wellbore Geometries for Geothermal Heat Mining Modeling Using CO_2.

Parameter	Unit	Value
Reservoir and Wellbore Geometries		
Injection Well Depth (H_0)	m	2500
Production Well Depth (H_1)	m	2150
Reservoir Depth (H_2)	m	500
Reservoir Length and Width ($2L_0$)	m	4000
Well Distance (L_1)	m	500
Injection Well Diameter	m	0.64
Production Well Diameter	m	0.32

Table 2

Input Parameter and Initial Values for Geothermal Heat Mining Modeling Using CO_2.

Parameter	Unit	Value
Reservoir Characteristics		
Reservoir Porosity	-	0.1
Reservoir Permeability	mD	30
Rock Specific Heat	J/(kg·K)	920
Rock Thermal Conductivity	W/(m·K)	2.51
Parameters for Relative Permeability		
Residual Gas Saturation	-	0.01
m_{VG}	-	0.65
Residual Liquid Saturation	-	0.05
Saturated Liquid Saturation	-	1.00
Parameters for Capillary Pressure		
Residual Liquid Saturation	-	0.03
m_{VG}	-	0.4118
Alpha	Pa^{-1}	6.08×10^{-5}
Maximum Capillary Pressure	Pa	6.40×10^{7}
Saturated Liquid Saturation	-	1.00
Reservoir and Injection Well Initial Conditions		
Reservoir Initial Fluid	-	Water
Reservoir Initial Temperature	℃	225
Reservoir Initial Pressure	MPa	20-25
CO2 Temperature at Injection Well Head	℃	30
CO2 Injection Mass Flow Rate	kg/s	30

A high temperature research version of T2Well/ECO2N software was provided by Lawrence Berkeley National Laboratory to perform this study. The wellbore modeling is governed by 1-D momentum equation, while 3-D flow in the multiple layers porous reservoir is governed by a multiphase version of the Darcy's Law. For these two subdomains, the mass and energy balance equations are solved together so that both reservoir and wellbores behaviors are coupled.

The simulation ran for a period of 30 years with the reservoir geometries presented in Table 1. Table 2 lists the initial parameter values of reservoir characteristics and conditions. The pressure gradient in reservoir will be 1 MPa per 100 m with the initial reservoir head pressure of 20 MPa. Along the injection wellbore, a linear temperature distribution of 30 ℃ to 225 ℃ is assumed. The injection wellhead conditions of CO_2 injecting mass flow rate of 30 kg/s and injecting temperature of 30 ℃ are set to be fixed.

To get the expected high CO_2 saturation flow from the production well, the simulation is set to be controlled by small production rate of 0.1 kg/s at the start-up. The CO_2 plume is formed and move toward to production wells. Meanwhile, due to the near-zero production rate, the pressure of the reservoir increases. When the pressure at the reservoir top at $R = 500$ m reaches 27 MPa which is 7 MPa higher than the reservoir top initial pressure, the production well is fully opened and the production is controlled by this reservoir head pressure (Fig. 4).

2.2 Simulation Results

The geothermal heat mining simulation results are presented in this section. The production will reach relatively steady state after 10 years. The CO_2 flow rate, pressure and temperature are able and reseanable to be considered as constants along the rest 20 years production. A CO_2-H_2O separator is necessary (Fig. 1) due to the two phase flow production which is indicated in Fig. 4. A CO_2 production rate of 22.5 kg/s for each production well or a total produced CO_2 mass flow rate of 90 kg/s is also reasonable to be used for the ORC working fluid selection analyses based on the results shown in Fig. 4. Similarly, produced CO_2 pressure of 22.5 MPa and temperature of 195 ℃ from Fig. 5 are taken into account for the following analyses and discussions.

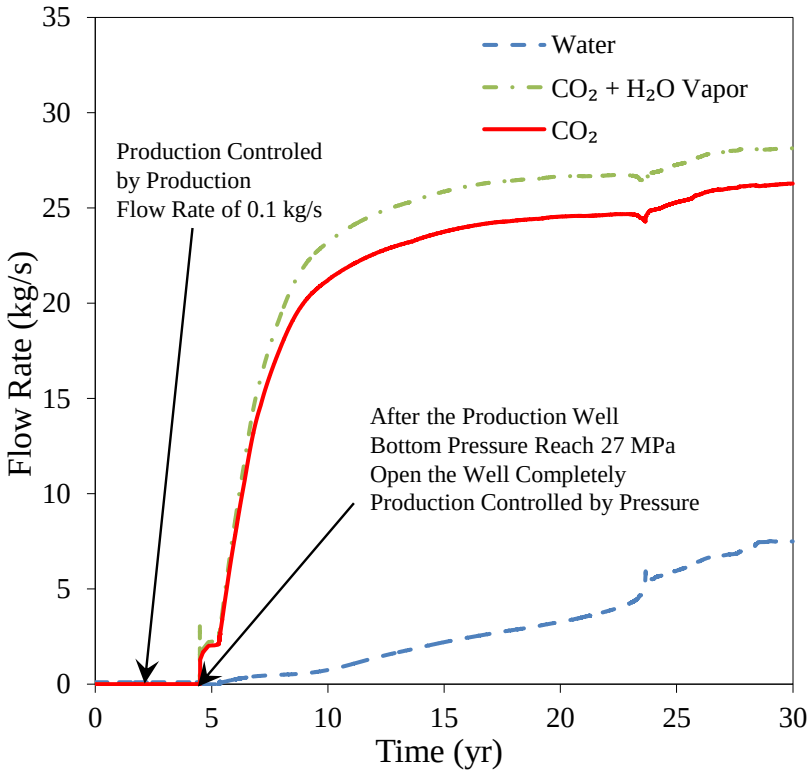

Fig. 4. Predicted Production Species and Flow Rates Over 30 Years.

Fig. 5 a) indicates the production well head pressure is more than 5 MPa larger than the injection well head pressure during steady production which makes elimitating CO_2 compressor for reinjection possible. In addition, the pressure drops of hot sCO_2 passing through the CO_2-H_2O separator and the evaporator can be ignored due to this large pressure difference between the injection well and the production wells which was recognized as the thermosiphon effect in CPG [8].

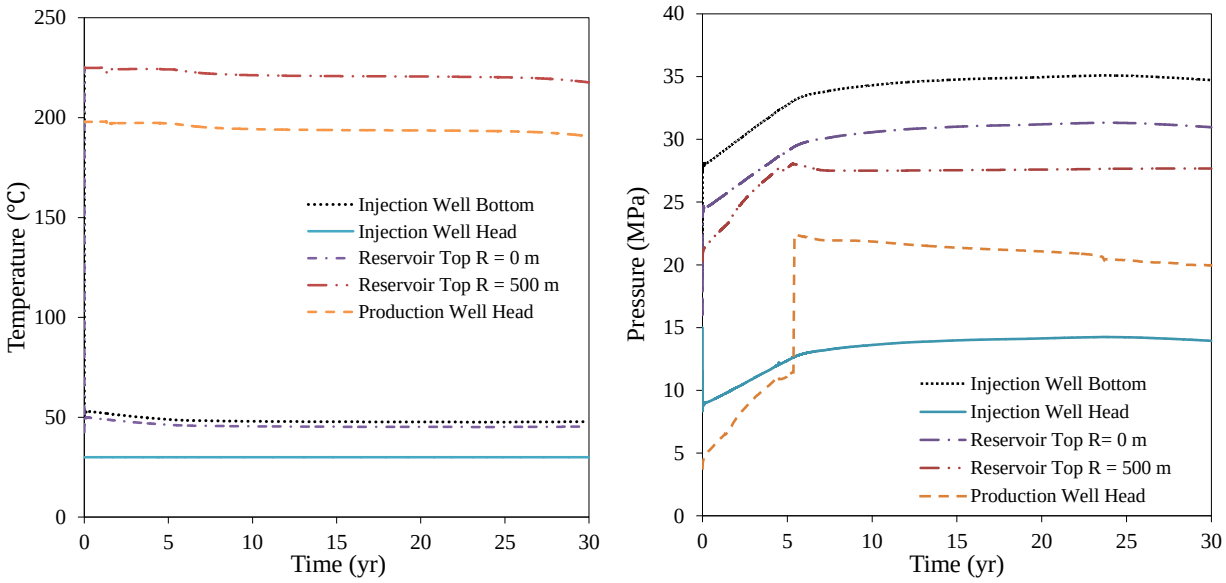

Fig. 5. a). Predicted Pressure in Wellbore and Reservoir Over 30 Years (Left); b). Predicted Temperature in Wellbore and Reservoir Over 30 Years (Right).

3. Organic Rankine Cycle Electric Power Generation Using Hot Produced sCO_2 from a Geothermal Reservoir

3.1 ORC Using Hot Produced sCO_2 Thermodynamic Model

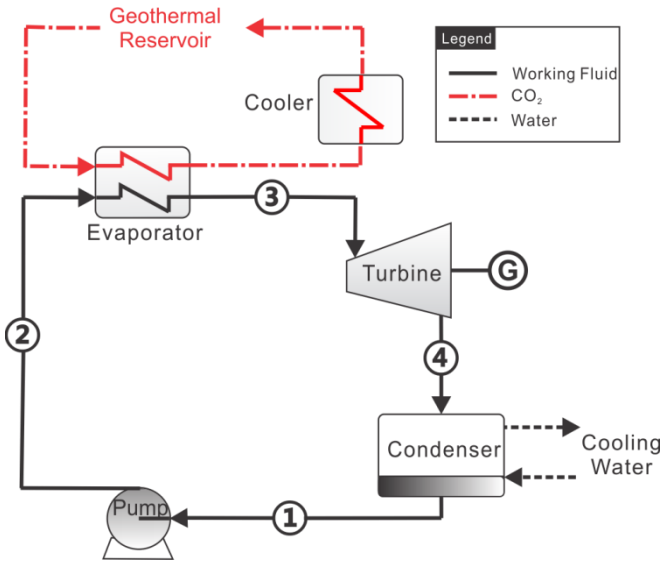

Fig. 6. System Diagram of Simple ORC.

The simple ORC which is illustrated in Fig. 6 was used to perform the working fluid selection analyses. Simple ORC system consists of evaporator, turbine, condenser and pump. For this particular case, the hot produced sCO_2 transfers heat to working fluid in the evaporator, then is cooled and re-injected back to the geothermal reservoir. The working fluid starts to be pumped at state 1 in Fig. 6 to operation pressure. The pressurized working fluid passes through the evaporator to be heated up then expands through the turbine to generate power. Then, the working fluid is cooled down from state 4 by cooling water.

The model and mathematic equations for each component used for ORC thermodynamic analysis are as follows.

Evaporator

The evaporator is the main component for this analysis connecting hot produced sCO_2 and working fluid. Since the evaporative pressure and mass flow rate of working fluid are undetermined, a model has been developed to obtain the optimum working fluid mass flow rate.

The energy balance of the evaporator is:

$$\dot{m}_{WF}\left(h_3 - h_2\right) = \dot{m}_{CO_2}\left(h_{CO_2,in} - h_{CO_2,out}\right) \tag{1}$$

$h_{out,evp}, h_{in,evp}$ are corresponding to evaporator outlet temperature and condenser temperature of working fluid. The CO_2 temperature at evaporator outlet is able to be calculated by equation (1) with an assumed working fluid mass flow rate. Furthermore, the temperature distribution in evaporator can be obtained by:

$$\dot{m}_{WF}\left(h_{WF,i+1} - h_{WF,i}\right) = \dot{m}_{CO_2}\left(h_{CO_2,i+1} - h_{CO_2,i}\right) \tag{2}$$

where $\sum_i \left(h_{WF,i+1} - h_{WF,i}\right) = h_3 - h_2$, $\sum_i \left(h_{CO_2,i+1} - h_{CO_2,i}\right) = h_{CO_2,in} - h_{CO_2,out}$. i is the mesh point of evaporator. Consequently, the pinch temperature in evaporator can be obtained. Then, the optimum working fluid mass flow rate is calculated through iteration.

The heat transferred from sCO_2 to the working fluid can be calculated by:

$$Q_{evp} = \dot{m}_{WF}\left(h_3 - h_2\right) \tag{3}$$

Pump

The process 1 – 2 in Fig. 6 is the isentropic compression. The pump work and isentropic efficiency are defined as:

$$W_p = \dot{m}_{WF}\left(h_2 - h_1\right) \tag{4}$$

$$\eta_{p,s} = \frac{h_{2s} - h_1}{h_2 - h_1} \tag{5}$$

Turbine

The isentropic expansion work and efficiency (states 3 to 4 in Fig. 6) in the turbine can be obtained by:

$$W_t = \dot{m}_{WF}\left(h_3 - h_4\right) \tag{6}$$

$$\eta_{t,s} = \frac{h_3 - h_4}{h_3 - h_{4s}} \tag{7}$$

Condenser

The heat ejected by the condenser is:

$$Q_{cond} = \dot{m}_{WF}\left(h_4 - h_1\right) \tag{8}$$

Cycle Performance

The system net power output can be obtained:

$$W_{net} = W_t - W_p \tag{9}$$

The ORC thermal efficiency can be calculated by equation (10) with the control volume shown in Fig. 7:

$$\eta_{ORC,th} = \frac{W_{net}}{Q_{evp}} \tag{10}$$

The thermal efficiency, also known as the 1st law efficiency, will not evaluate the quality of the energy conversion process and reflect the potential for improvement. The exergy efficiency, which will answer these questions, is defined as:

$$\eta_{ex} = \frac{W_{net}}{\sum \dot{m}_{in} e_{in} - \sum \dot{m}_{out} e_{out}} \tag{11}$$

where

$$e = \left(h - h_0\right) - T_0\left(s - s_0\right) + \frac{V^2}{2} + g\Delta H \tag{12}$$

In this analysis, there are no change in kinetic and potential energy, equation (12) can be reduced to

$$e = \left(h - h_0\right) - T_0\left(s - s_0\right) \tag{13}$$

where T_0, h_0, s_0 are the temperature, enthalpy and entropy of the working fluid at the reference state which is 0.1 MPa, 25 ℃ in this paper.

The specific net power output can be calculated by:

$$w_{net} = \frac{W_{net}}{\dot{m}_{WF}} \tag{14}$$

.

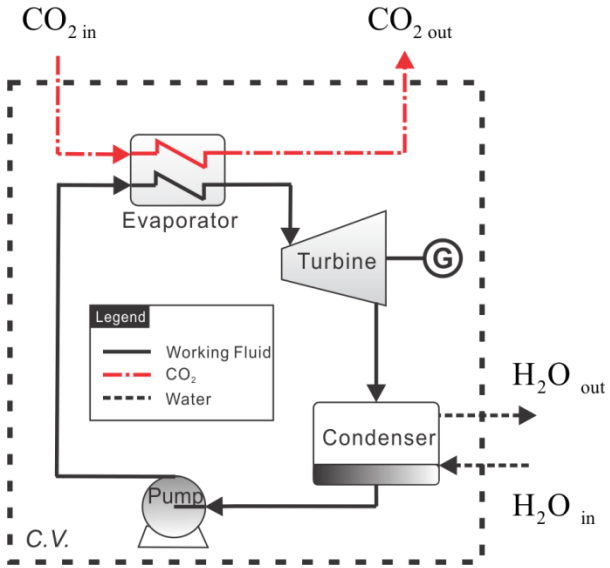

Fig. 7. Control Volume for ORC Exergy and Thermal Efficiency Calculation.

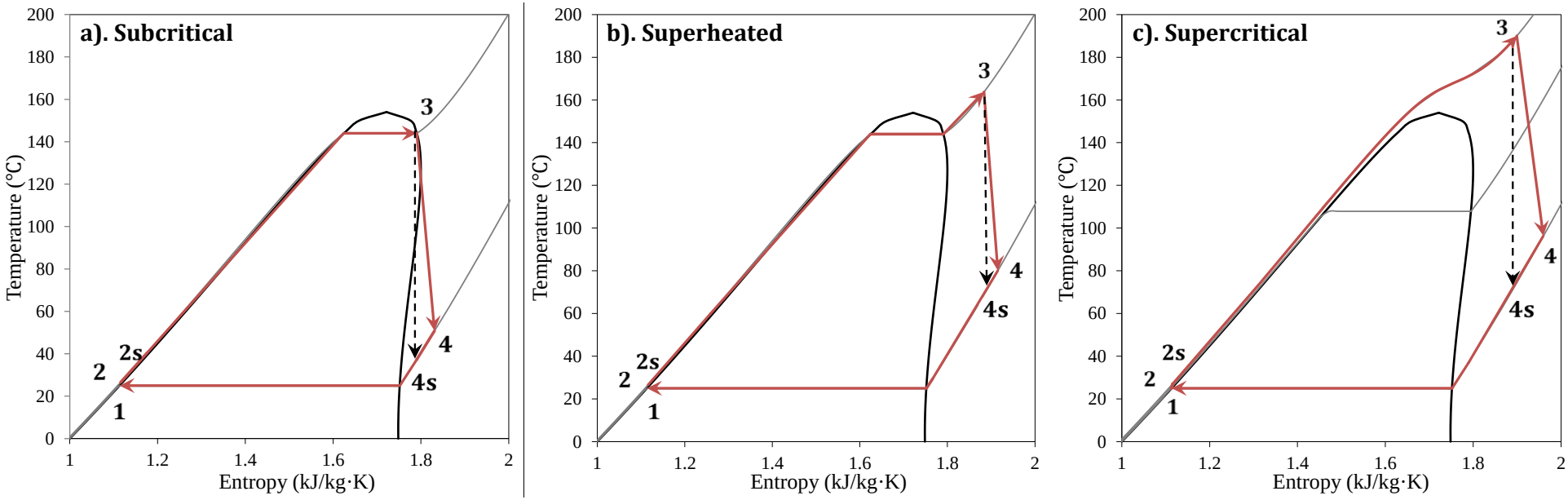

Fig. 8. *T-s* diagrams for Three Approaches of Simple ORC; a). Subcritical ORC (Left); b). Superheated ORC (Middle); c). Supercritical ORC (Right).

In this paper, three different types ORC are discussed: subcritical, superheated and supercritical approaches (Fig. 8). The input parameter values and assumptions are listed in Table 3. All properties data are obtained from the NIST REFPROP data base.

Table 3

Parameter Values of Working Fluid Selection and ORC Power Generation Analyses.

Parameter	Unit	Value
Hot Produced CO_2 Flow Rate	kg/s	90
Hot Produced CO_2 Temperature	℃	195
Hot Produced CO_2 Pressure	MPa	22.5
CO_2 Cooler Outlet Temperature	℃	30
Turbine Isentropic Efficiency η_t	%	88
Pump Isentropic Efficiency η_p	%	85
Condenser Temperature T_{cond}	℃	25
Maximum Evaporative Temperature for Subcritical ORC	℃	T_{cr} -5
Upper Limit of Supercritical Pressure	MPa	10
Condenser Minimum Temperature Approach $T_{cond,pinch}$	℃	3
Evaporator Cold Inlet and Hot Outlet Minimum $\Delta T_{evp,\min}$	℃	5
Evaporator Minimum Temperature Approach $T_{evp,pinch}$	℃	3

3.2 Demonstration of the Model with R600 as Working Fluid

To demonstrate the calculation and optimization processes of working fluid selection, R600 ($T_{cr}=151.98$ ℃, $p_{cr}=3.796$ MPa) is selected since it is classified as dry working fluid which would be feasibly applied to all three ORC approaches. In this analysis, the enthalpy change in the working fluid pump is ignored. The pressure drops on both working fluid side and sCO_2 side are also neglected in the evaporator.

The heat source conditions for all three ORC approaches, which are the produced sCO_2 mass flow rate, temperature and pressure from a geothermal reservoir shown in Table 3, can be obtained from section 2 and fixed in the flowing analyses and calculations.

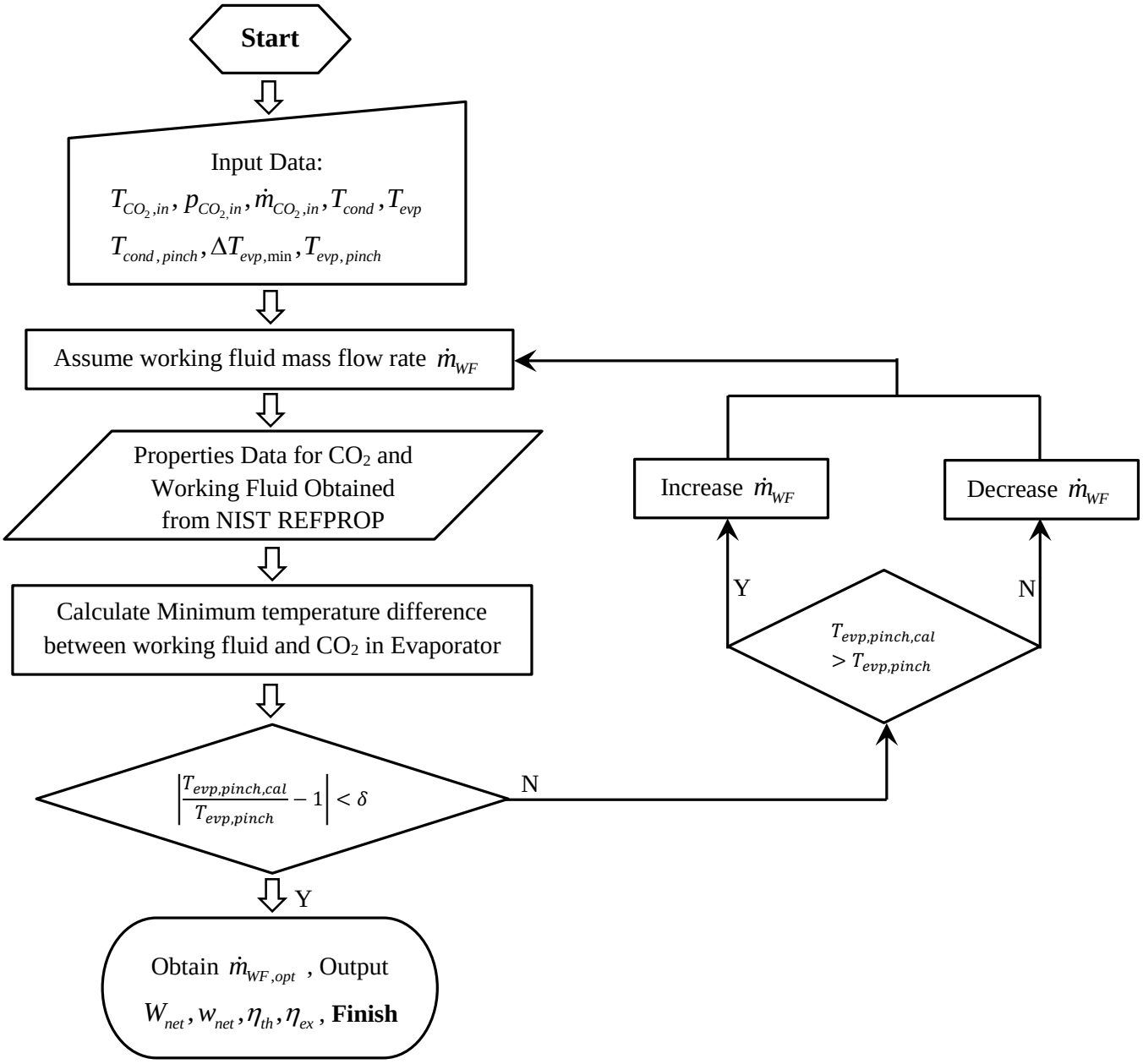

Fig. 9. Flow Chart of the Procedure to Obtain Optimum Working Fluid Mass Flow Rate.

For subcritical and superheated approaches, the evaporative temperature and working fluid mass flow rate need to be determined; for supercritical approach, the supercritical pressure, i.e. the working fluid pressure at pump outlet, as well as the working fluid mass flow rate should be determined. The constraint for the optimum working fluid mass fluid calculation is the pinch temperature in the evaporator. The procedure to get the optimum working fluid flow rate is presented in Fig. 9 for a given evaporative temperature or supercritical pressure.

3.2.1 Subcritical ORC

The *T-s* diagram of subcritical ORC in Fig. 8 a) shows the evaporative temperature is below the critical point. Meanwhile, at the evaporator outlet, the working fluid is saturated vapor. The maximum evaporative temperature is assumed as 5 ℃ below the critical temperature in this analysis. Fig. 10 presents that the optimum working fluid mass flow rates of 49.51 kg/s, 56.50 kg/s and 66.19 kg/s are obtained at the evaporative temperature of 125.23 ℃, 100.23 ℃ and 75.23 ℃ respectively for R600. The pinch point occurs at the evaporator bubble point. For R600, the higher the evaporative temperature reaches, the less energy needed for evaporating and less exergy loss will be with the optimum R600 mass flow rate to get the pinch temperature of 3 ℃. However, the exergy destruction increases which is also reflected in the ORC exergy efficiency decrease shown in Table 4.

3.2.2 Superheated ORC

Similarly as the subcritical approach, the evaporative temperature of superheated approach is also below the critical point but the saturated vapor will continuously be heated up (Fig. 8 b)). The maximum evaporative temperature for superheated approach is also 5 ℃ below the critical temperature. Unlike subcritical approach, the working fluid vapor will be at superheated state then goes through the turbine to generate power. Potentially, the superheated approach will have higher turbine inlet temperature compared to the subcritical approach to achieve larger net power output. However, the optimum working fluid flow rate is relatively small compared to the subcritical approach. It can be seen from Table 4 that at the same evaporative temperature and pressure, subcritical approach will generate more power than superheated approach for R600. This indicates the ORC thermodynamic performance is not simply monotone with only one

factor. Fig. 11 shows the exergy destruction is getting large with the decreasing of evaporative temperature from 140.48 ℃ to 115.48 ℃. However, it is not necessary for the net power output to decrease. On the contrary, the maximum net power output would not be achieved with the maximum thermal efficiency or exergy efficiency. The optimum result will be presented in the following discussion.

3.2.3 Supercritical ORC

The evaporator pressure of supercritical ORC approach is above critical point which the flow in the evaporator will not cross the two phase region (Fig. 8 c)). Fig. 12 shows the pressure of R600 at pump outlet increases and gets far away from the critical point, the exergy loss and exergy destruction decrease which results in the exergy efficiency increases. When the supercritical pressure is near critical point, the properties of working fluid will dramatically change where the pinch point will occur (Fig. 12). The more "parallel" temperature distribution curves of both working fluid side and CO_2 side appear at a larger supercritical pressure for R600. In Table 4, it shows more power is generated at higher supercritical pressure. Nevertheless, high system pressure requires high pressure bearing capacity of the infrastructure which will significantly affect cost of the system. Therefore, the cost analyses are also necessary for the future work.

Table 4

Thermodynamic Results Corresponding to Fig. 10, Fig. 11 and Fig. 12.

	T_{evp} **(℃)**	$\dot{m}_{WF,opt}$ **(kg/s)**	W_{net} **(MW_e)**	$\eta_{ORC,th}$ **(%)**	$\eta_{ORC,ex}$ **(%)**	w_{net} **(kW_e/(kg/s))**
Subcritical	125.23	49.51	3.9578	16.6	69.1	79.95
	100.23	56.50	3.6948	14.2	62.3	65.40
	75.23	66.19	3.1001	10.9	50.9	46.84
Superheated	140.48	23.91	2.7594	17.8	63.3	115.42
	115.48	27.49	2.8482	15.4	58.3	103.61
	90.48	32.13	2.7209	12.3	50.3	84.69
	p_{scrit} **(MPa)**	$\dot{m}_{WF,opt}$ **(kg/s)**	W_{net} **(MW_e)**	$\eta_{ORC,th}$ **(%)**	$\eta_{ORC,ex}$ **(%)**	w_{net} **(kW_e/(kg/s))**
Supercritical	4.296	23.47	2.7666	19.2	47.6	117.89
	6.296	29.12	3.0479	19.8	69.3	104.68
	8.796	40.02	3.7318	19.4	72.9	93.25

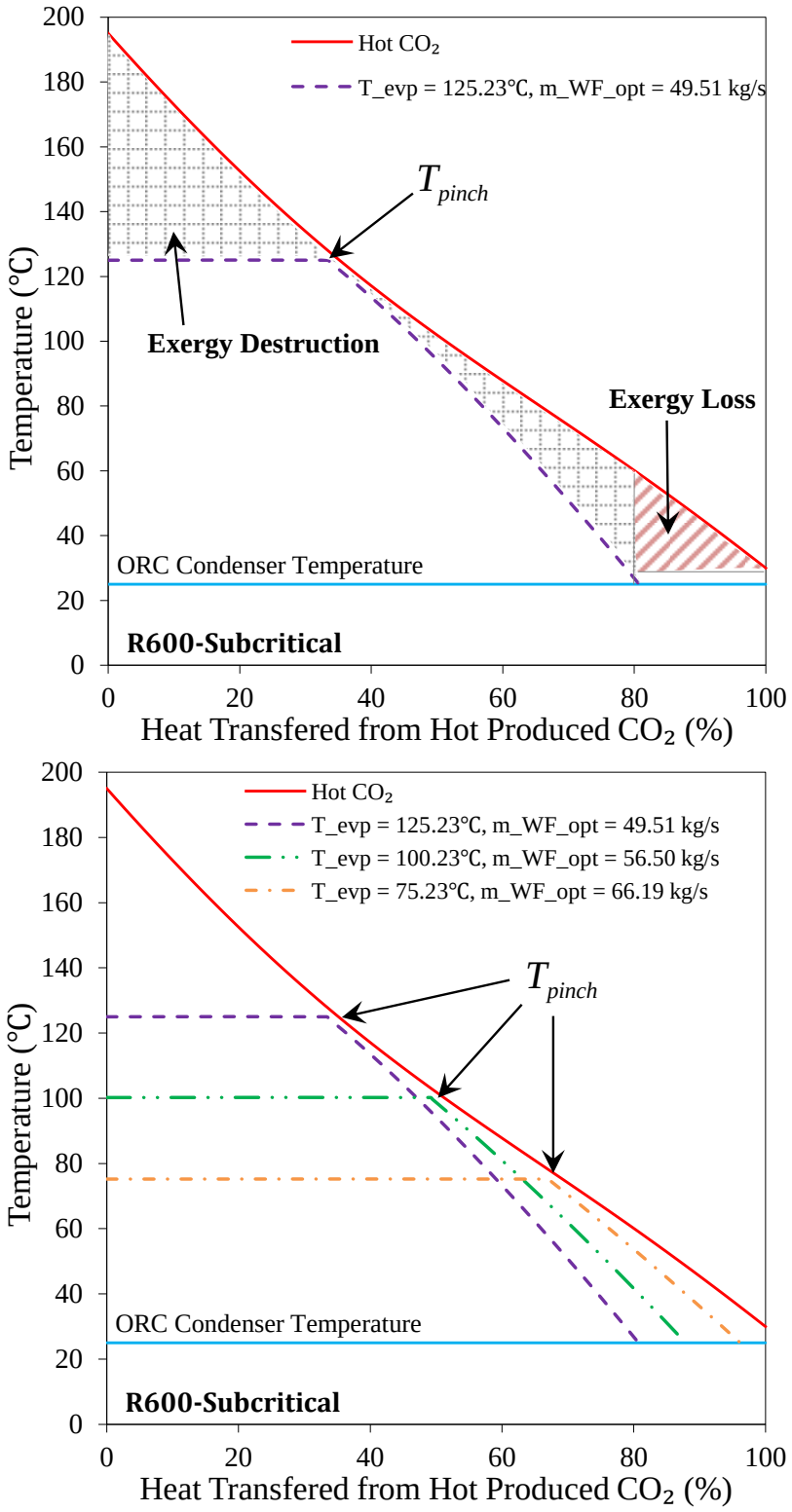

Fig. 10. Subcritical ORC Optimum OF Mass Flow Rates with R600 as Working Fluid at Different Evaporative Temperatures.

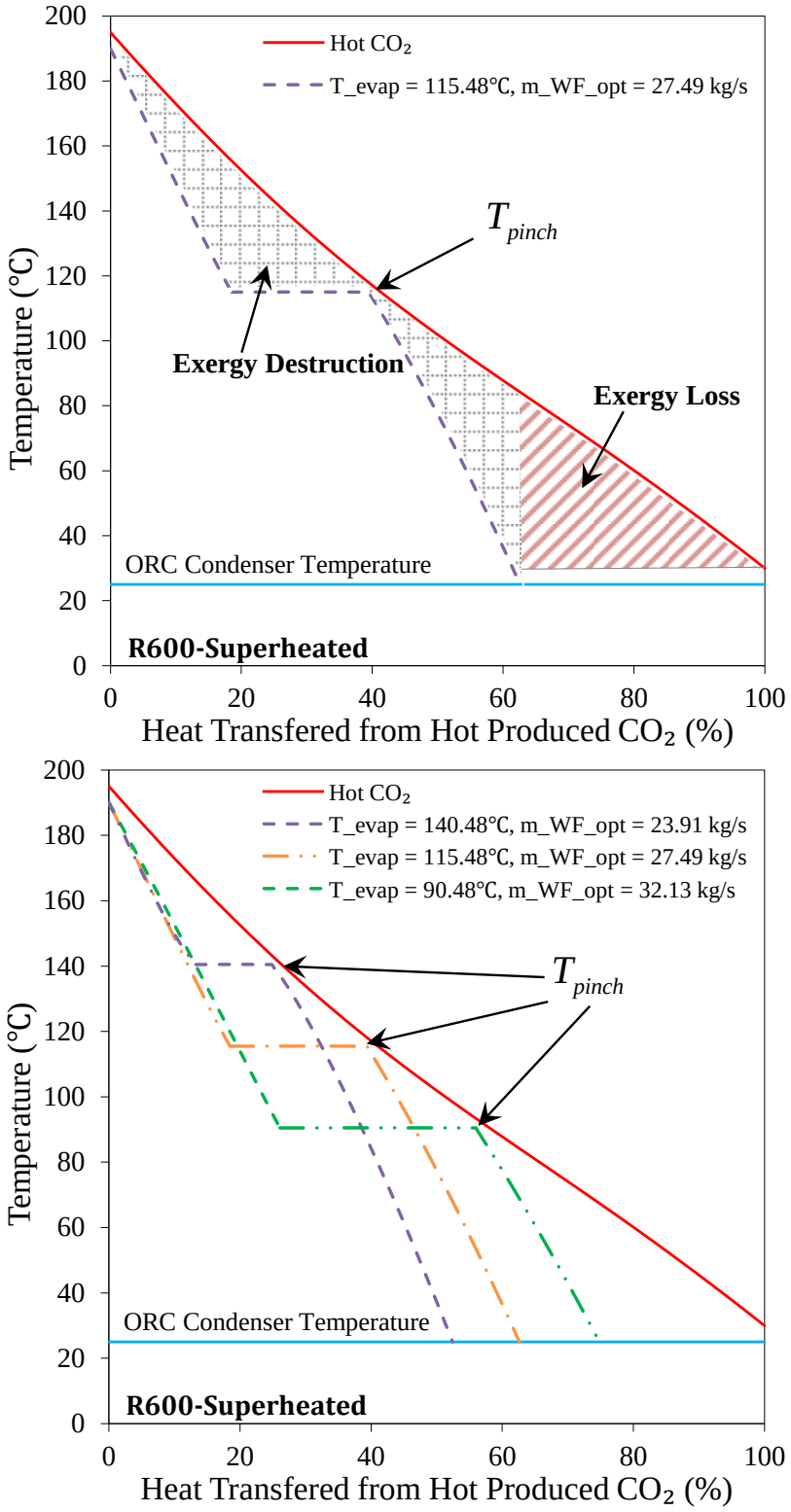

Fig. 11. Superheated ORC Optimum OF Mass Flow Rates with R600 as Working Fluid at Different Evaporative Temperatures.

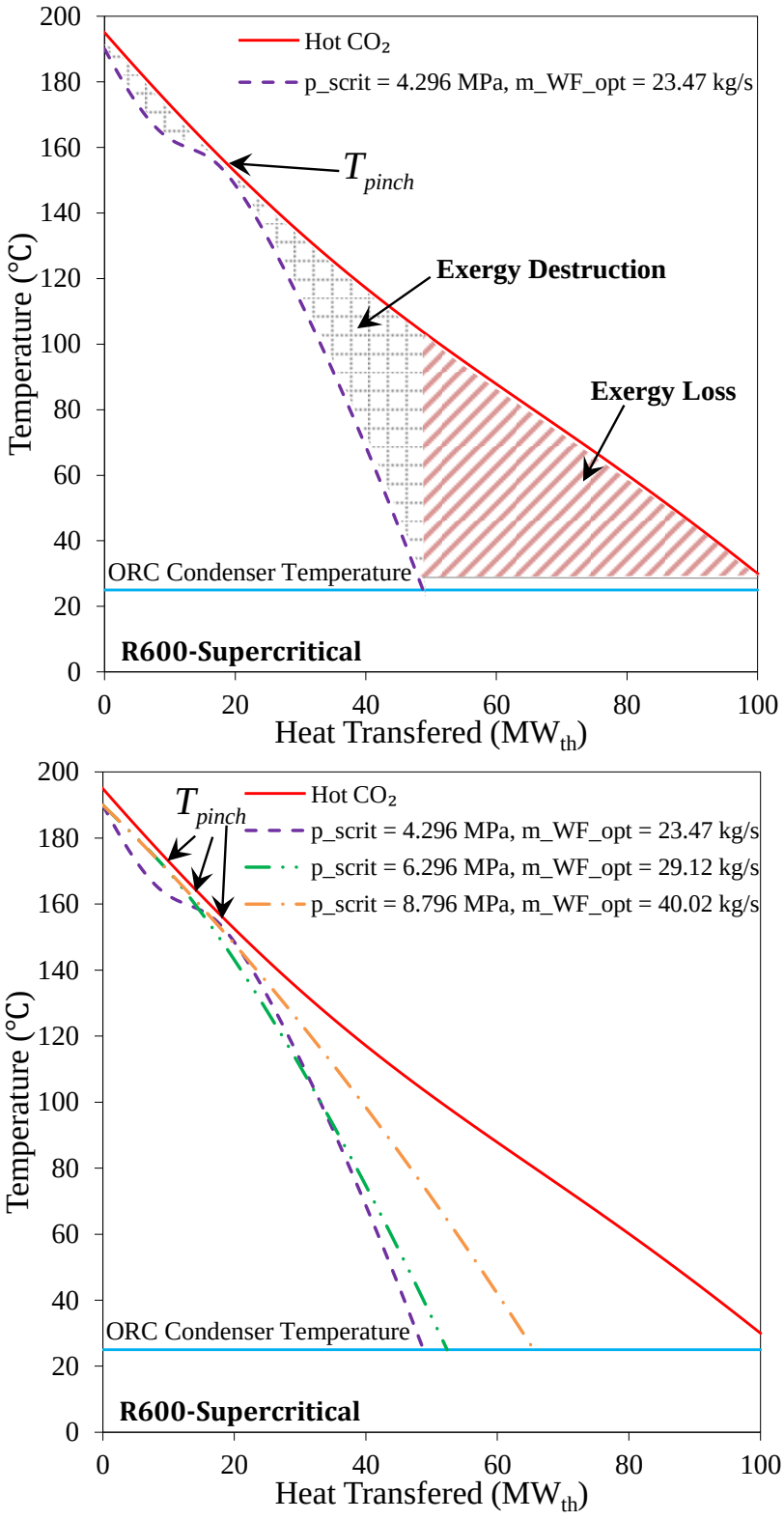

Fig. 12. Supercritical ORC Optimum OF Mass Flow Rates with R600 as Working Fluid at Different Supercritical Pressures.

3.2.4 Model Validation and Optimized Results

An ASPEN Plus model has been established to validate the calculated results of the three ORC models. The ORC thermal efficiency and net power output presented in Fig. 13 show a very good agreement between the ASPEN Plus model and the thermodynamic model created in this paper.

The net power output, optimum working fluid flow rate, ORC thermal efficiency, ORC exergy efficiency and specific net power output are the factors have been calculated and considered for working fluid selection. Since the ORC thermodynamic performance is related to many factors, such as physical properties of working fluids, heat source types and ambient conditions, it is not practical to get the most optimum design considering for all factors. Therefore, for each working fluid, the maximum net power output would be the objective for optimization.

The different evaporative temperatures for the subcritical ORC and superheated ORC with R600 as working fluid have been considered. For the supercritical ORC approach, the supercritical pressures of 0.5 to 5 MPa over the critical pressure have been used for simulation.

The results plotted in Fig. 13 indicate the maximum net power output and ORC thermal efficiency for subcritical approach are achieved at the possible largest evaporative temperature which is 125.23 ℃ for R600. The optimum net power output of 3.9578 MW_e and $\eta_{ORC,th}, \eta_{ORC,ex}, w_{net}$ have been calculated. The maximum net power output is calculated out of 2.8434 MW_e, for superheated approach appears at the evaporative temperature of 116.98 ℃. For supercritical approach of R600, the maximum net power output of 3.9578 MW_e is obtained at the largest possible supercritical pressure of 10 MPa which is also the assumed largest evaporator pressure for all working fluids. Similarly, this procedure will be followed for performing analyses of all possible working fluids presented in this paper. In addition, the comparisons of calculation results for all working fluids will then consider factors besides net power output.

It needs to be mentioned that the pre-selection criteria discussed in section 4 have to be considered in this demonstration calculation and optimization. The pre-selection criteria are discussed in detail as follows.

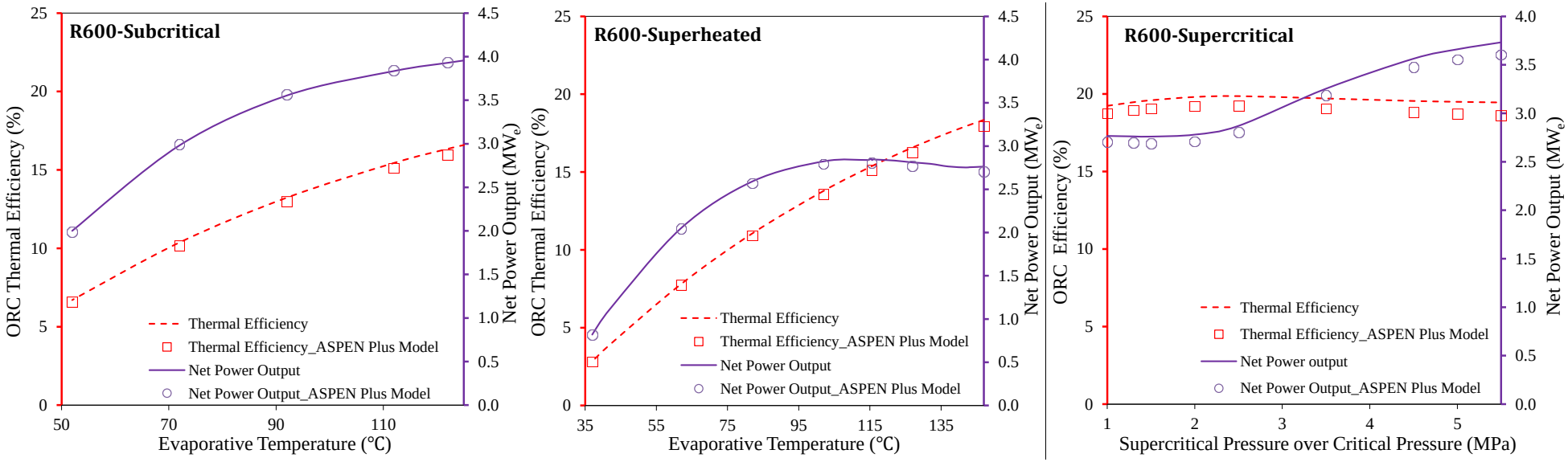

Fig. 13. Thermodynamic Results for a). Subcritical, b). Superheated and c). Supercritical Approaches with R600 as Working Fluid.

Table 5

Optimum Calculation Results for R600.

	T_{evp} **(℃)**	$\dot{m}_{WF,opt}$ **(kg/s)**	W_{net} **(MW_e)**	$\eta_{ORC,th}$ **(%)**	$\eta_{ORC,ex}$ **(%)**	w_{net} **(kW_e/(kg/s))**
Subcritical	125.23	49.51	3.9578	16.6	69.1	79.95
Superheated	116.98	27.20	2.8434	15.5	58.6	104.52
	p_{crit} **(MPa)**	$\dot{m}_{WF,opt}$ **(kg/s)**	W_{net} **(MW_e)**	$\eta_{ORC,th}$ **(%)**	$\eta_{ORC,ex}$ **(%)**	w_{net} **(kW_e/(kg/s))**
Supercritical	10.00	42.23	3.8429	19.4	77.4	91.00

4. ORC Thermodynamic Model and Organic Working Fluid Pre-selection Criteria

4.1 Type of Organic Working Fluid

The organic working fluids can be classified as three types based on the slope of saturated vapor curve of the working fluids: dry fluid, isentropic fluid and wet fluid (Fig. 14).

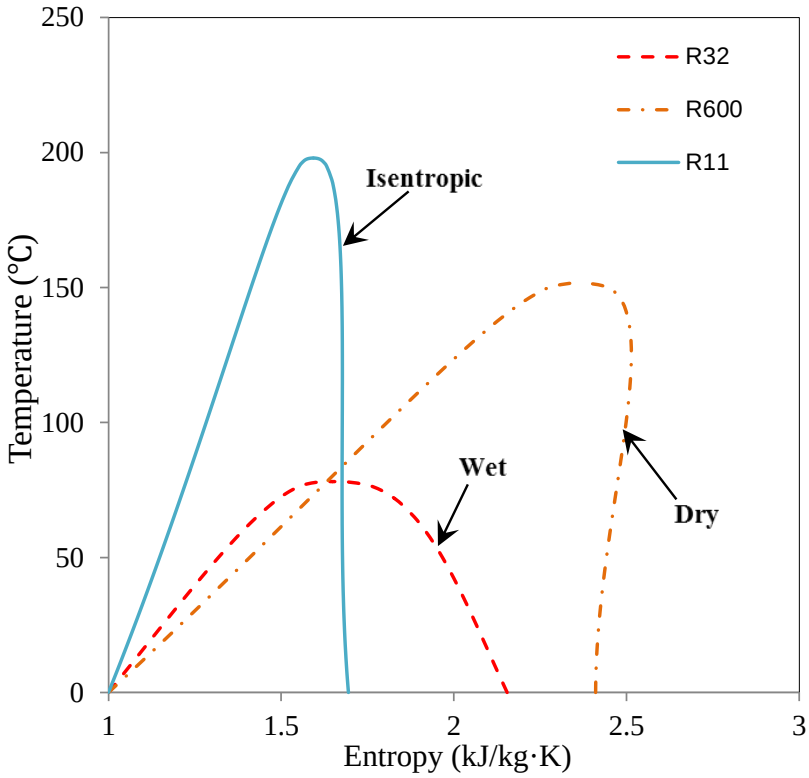

Fig. 14. Three Types of Organic Working Fluid.

A method used to determine these three types of organic working fluids was firstly proposed by Liu et al. [20]. An equation was derived and ξ, the slope of the saturation vapor curve was defined and calculated:

$$\xi = \frac{ds}{dT_H} \tag{15}$$

When $\xi > 0$, the fluid is dry fluid; when $\xi < 0$, the fluid is dry fluid and if $\xi \approx 0$, the working fluid is isentropic fluid. However, the Liu et al. used ideal gas relations to derive an equation to predict ξ:

$$\xi = \frac{ds}{dT_H} = \frac{c_p}{T_H} - \frac{\frac{n \cdot T_{rH}}{1-T_{rH}} + 1}{T_H^2} \Delta h_H \tag{16}$$

where T_H is normal boiling point indicated by the authors; Δh_H is enthalpy change of evaporation; c_p is specific heat; $T_{rH} = T_H / T_{cr}$.

Another parameter σ called molecular complexity was introduced and defined as:

$$\sigma = \frac{T_{cr}}{R}\left(\frac{\partial s}{\partial T}\right)_{sv,T=0.7T_{cr}} \tag{17}$$

The author also calculated the value of σ by adopting the ideal gas law. This paper claims "the qualitative effects of the molecular structure on the value of σ are easily highlighted in case of the saturated vapor is comparable to an ideal gas" and equation (17) was derived to predict the slope of the saturated vapor curve [21]:

$$\begin{aligned}\sigma &= \frac{T_{cr}}{R}\left[\left(\frac{\partial s}{\partial p}\right)_T \left(\frac{\partial p}{\partial T}\right)_{sv} + \left(\frac{\partial s}{\partial T}\right)_p\right]_{sv,T=0.7T_{cr}} \\ &= \frac{T_{cr}}{R}\left[-\frac{R}{p}\left(\frac{\partial p}{\partial T}\right)_{sv} + \frac{C_p}{T}\right]_{sv,T=0.7T_{cr}} \\ &= \left[-\frac{1}{p_R}\left(\frac{\partial p_r}{\partial T_r}\right)_{sv} + \frac{\gamma}{\gamma-1}\frac{1}{T_r}\right]_{sv,T=0.7T_{cr}}\end{aligned} \tag{18}$$

The equations (16) and (18) were widely used to classify the types of the working fluid for ORC. However, the ideal gas law would fail near the saturated vapor curve, especially closed to the critical point. Therefore the predictions are not accurate enough to divide isentropic working fluids. To explain this more convinced, the calculations of specific volume of R600 using the ideal gas law and saturated vapor properties respectively are performed. For the ideal gas, the specific volume can be calculated by:

$$\upsilon = \frac{RT}{pM} \tag{19}$$

where υ is the specific volume in unit of m^3/kg; T is the ideal gas temperature in unit of K; p is the ideal gas pressure in unit of kPa; M is the molecular weight in unit of kg/kmol; R is the gas constant of 8.314 kJ/kmol·K. The specific volume of R600 at the pressure of 0.25 MPa, 0.5 MPa, 1 MPa and 3MPa at the saturated vapor conditions were calculated by equation (19). The error between calculated value by ideal gas law and real value is defined as:

$$\upsilon_{error} = \frac{\upsilon_{cal} - \upsilon_{real}}{\upsilon_{real}} \times 100\% \tag{20}$$

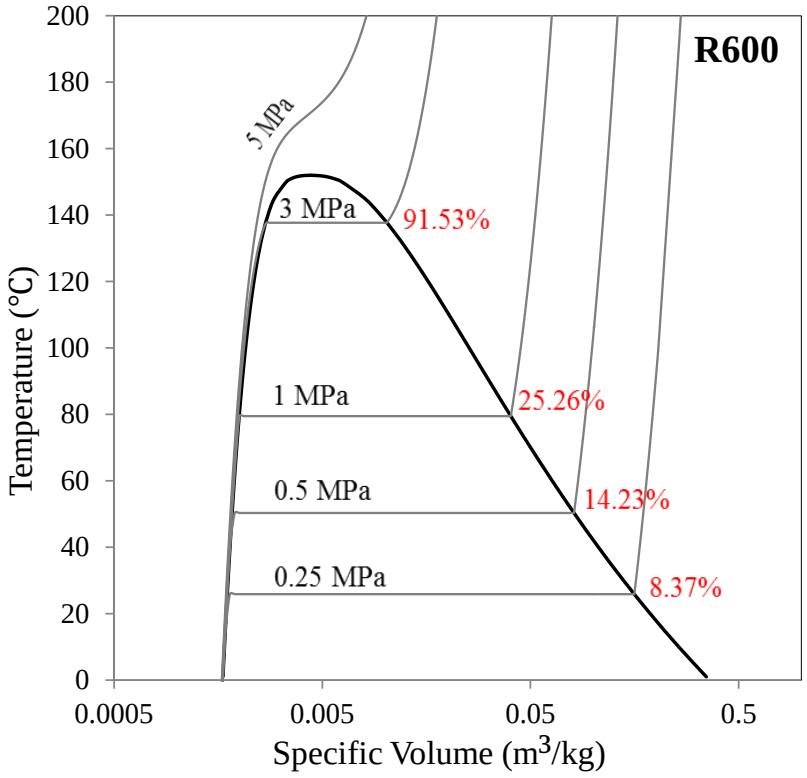

Fig. 15. $T-\upsilon$ Diagram of R600 and Specific Volume Error on Saturated Vapor Curve of Different Pressure.

The errors are shown in Fig. 15. If the saturated vapor pressure is lower to 0.1 MPa, the error is 8.37% which is already a significant shift. If the working fluid pressure is at the ORC operation conditions (for example $0.7\,p_{cr}$), the error will not be acceptable. The region that the vapor can be

treated as ideal gas is far from the saturated vapor curve. Thus, the ideal gas law will fail for working fluids classification to calculate ξ and σ. Therefore, the more accurate way to calculate the slop of saturated vapor curve would be using the actual physical properties.

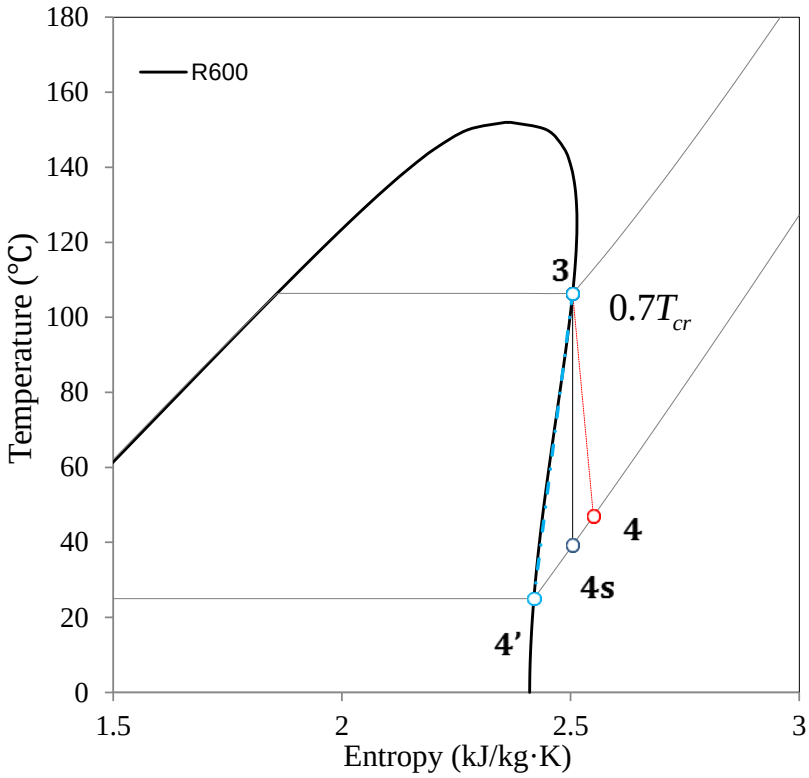

Fig. 16. *T-s* Diagram of Illustration of Fluid Type Classification.

A method to classify working fluids for ORC has been proposed. The evaporative temperature of $0.7T_{cr}$ at state 3 in Fig. 16 is picked to perform the analysis. State 3 to 4s is isentropic process; State 3 to 4 is turbine expansion process with isentropic efficiency of 95%. State 4' is saturated vapor at condenser temperature. An equation is defined to determine the working fluid type:

$$\varepsilon = \frac{s_{4s} - s_{4'}}{s_4 - s_{4s}} \tag{21}$$

ε is defined as working fluid type factor in this paper. $s_4, s_{4'}, s_{4s}$ are the entropy values of state 4, 4s and 4'. If $-1 \le \varepsilon \le 1$, the working fluid is isentropic fluid; If $\varepsilon < -1$, the working fluid is wet fluid; If $\varepsilon > 1$, it is dry fluid. Using this method, these thirty fluids types are determined and listed in Table 4.

4.2 Turning Points of Isentropic and Dry Working Fluids

Rayegan et al. stated a practical limit for a working fluid in ORC should be considered to avoid the presence of liquid in the turbine [16]. Potentially, for dry fluids and isentropic fluids, the liquid is also possible to be formed during the isentropic expansion for subcritical ORC, superheated ORC and supercritical ORC shown in Fig. 17.

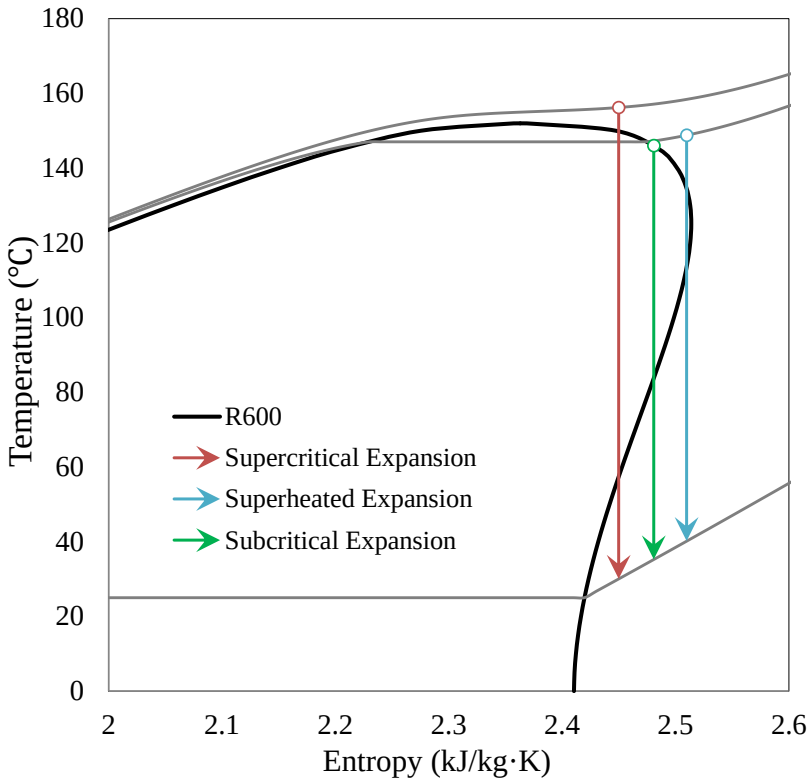

Fig. 17. Isentropic Expansion Process for Three ORC Approaches.

To prevent the erosion of turbine blades, a concept of "turning point" has been proposed. As mentioned in the section 4.1, the slope of saturated vapor curve can be expressed as equation (12). The turning point T_{tn} can be calculated by:

$$\xi = \left(\frac{\partial s}{\partial T} \right)_{sv, T=T_{tn}} = 0 \tag{22}$$

In Fig. 18, the turning point of R600 is 125.23 ℃. When the entropy value of working fluid smaller than $s_{T=125.23℃}$ and the working fluid temperature larger than 125.23 ℃ at the turbine inlet

for all three ORC approaches in the section 3.1, it is highly possible the fluid will be formed during expansion (Fig. 17). However, if the entropy value of working fluid smaller than $s_{T=125.23℃}$ and the working fluid temperature smaller than 125.23 ℃ at the turbine inlet, there is no chance of turbine blades erosion. Nevertheless, when the working fluid temperature at the turbine inlet is larger than its turning point, the turbine will be safe for all the three approaches.

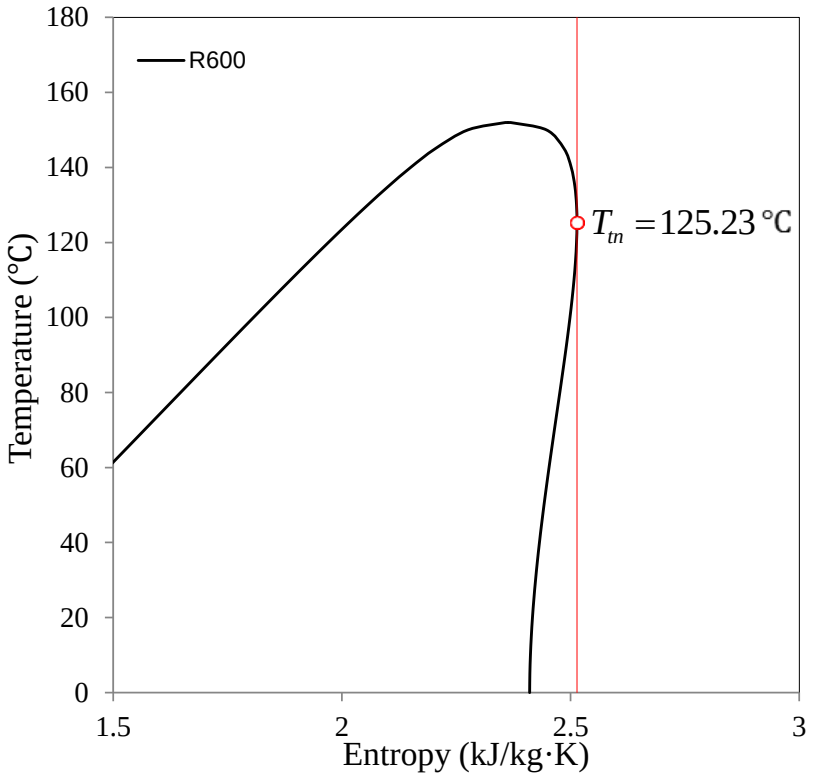

Fig. 18. Turning Point of R600.

4.3 Minimum Turbine Inlet Temperatures of Wet Working Fluids for fixed condenser Temperature

Besides the isentropic and dry working fluids selection criteria, a concept of minimum turbine inlet temperature of a wet working fluid is necessary to be defined and explained for the selection of wet working fluids. Similarly, to avoid fluid forming in the turbine expansion process, there should be a minimum turbine inlet temperature corresponding to the condenser temperature with the given evaporator pressure:

$$T_{t,in,\min} = T\left(s_{sv,cond}, p_{evp}\right) \tag{23}$$

In this analysis, the condenser temperature is fixed to 25 ℃. The corresponding $T_{t,in,\min}$ will be calculated to make sure the turbine inlet temperatures of ORC with wet working fluids feasible.

4.4 Potential Working Fluid Screening and Pre-selection

The potential working fluids with the critical temperature in the range of 50 ℃ to 225 ℃ are listed in Table 6. The environmental impacts, ozone depletion potential (ODP) and global warming potential (GWP) values from resources online are also presented. The ODP is a parameter that refers to the level that ozone depletion caused by a substance. The ODP of R11 is defined to be 1.0. The ODP for other substances are compared to R11 based on their abilities to deplete the ozone. The high ODP working fluid like R11, R114 have been assigning to be phased out by the Montreal and the Kyoto protocols since they are directly damaging the ozone. R11 and R114 production in U.S. have stopped in 1996. In consequence, the high ODP working fluid (ODP > 0.5 in this paper) will not be considered.

The GWP is a factor reflecting the effect of a substance. Similar as the ODP, the CO_2 with the GWP of 1 is the scale for comparisons with other substances. Typically, the time period of 100 years is used for evaluating the effect on the global warming over time. However, even the GWP of some working fluids shown in Table 6 are thousands times of CO_2, as the ORC working fluid which will not exhausted to atmosphere, the GWP will be a minor factor in working fluid selection.

NFPA 704 is a standard maintained by National Fire Protection Association in U.S. which is widely used to identify the flammability, health impact and chemical reactivity of a substance. The NFPA 704 codes for all potential working fluids in this paper are presented in Table 6. In this paper, concerning health impact and chemical reactivity which is a part of safety impacts, the substances with blue and yellow codes of equal or larger than 3 are removed from the list. Although flammability is also one aspect of safety, the substances with NFPA 704 red code 3, 4 are still considered since the flammable working fluids like R600/R601 are widely considered as ORC working fluids. However, at the similar magnitude of thermodynamic performance, the flammable working fluids should be avoided.

Table 6

Physical Properties, Environmental Impacts and Safety Data of Potential Working Fluids

Potential Working Fluid	Physical Properties				Environmental, Safety and Health Impact				
					Environmental		NFPA 704 Fire Diamond		
	T_{cr} (℃)	P_{cr} (MPa)	Fluid Type	Turning Point (℃)	ODP	GWP 100-yr Horizon	Flammability (Red)	Toxicity (Blue)	Instability (Yellow)
R11	197.96	4.408	Isentropic	118.78	1.0	4750	0	1	0
R113	214.06	3.392	dry	192.18	0.8	6130	0	1	0
R114	145.68	3.257	dry	121.13	1.0	10000	0	2	0
R115	79.95	3.129	dry	52.98	0.6	7370	0	1	0
R12	111.97	4.136	wet	-	1.0	10900	0	2	0
R123	183.68	3.662	dry	150.62	0.02	77	0	2	1
R124	122.28	3.624	dry	82.93	0.022	609	0	1	0
R125	66.02	3.618	wet	-	0	3500	0	1	3
R134a	101.06	4.059	wet	-	0	1430	1	2	0
R141b	204.35	4.212	Isentropic	166.11	0.12	725	1	2	0
R142b	137.11	4.055	Isentropic	73.99	0.07	2310	0	1	0
R143a	72.71	3.761	wet	-	0	4470	4	1	0
R152a	113.26	4.517	wet	-	0	124	4	2	0
R21	178.33	5.181	wet	-	0.04	151	0	1	0
R218	71.87	2.640	dry	55.51	0	8830	0	1	0
R22	96.15	4.990	wet	-	0.05	1810	0	2	1
R227ea	101.75	2.925	dry	82.56	0	3220	0	1	1
R236fa	124.92	3.200	dry	97.47	0	9810	0	1	0
R236ea	139.29	3.502	dry	122.93	0	1370	0	1	0
R245ca	174.42	3.925	dry	147.70	0	693	1	3	0
R245fa	154.01	3.651	dry	127.02	0	1030	1	2	0
RC318	115.23	2.778	dry	100.69	0	10300	0	2	0
R32	78.11	5.782	wet	-	0	675	4	2	1
R365mfc	186.85	3.266	dry	170.44	0	794	0	1	0
C_4F_{10}	113.18	2.323	dry	103.38	0	8860	0	1	0
C_5F_{12}	147.41	2.045	dry	141.17	0	9160	3	1	0
R600	151.98	3.796	dry	125.23	0	4	4	1	0
R600a	134.66	3.629	dry	107.79	0	4	4	1	0
R601	196.55	3.370	dry	179.40	0	0.1	4	1	0
R601a	187.20	3.378	dry	171.10	0	0.1	4	1	0

Based on the discussion above, the considerations for ORC working fluid pre-selection are as follows:

a. High ODP (> 0.5) fluids should be avoided, which are R11, R113, R114, R115, R12;
b. Toxic fluids which have the NFPA 704 blue code more than 2 shoud be avoided; Therefore, R245ca was removed from the list.
c. Instable fluids which have the NFPA 704 yellow code more than 2 should be avoided; As a consequnce, R125 was removed.
d. For subcritical ORC, the wet fluid would not work feasibly since the fluid formation during expansion in the turbine;
e. For subcritical ORC, the evaporative temperature should be equal or less than turning point to avoid fluid formation in turbine expansion.
f. For superheated and supercritical ORC, the turbine inlet tempearture of 190 ℃ used in this analysis should be larger than the minimum turbine inlet tmpreature of all wet working fluids in Table 6.

5. Results Comparison and Discussion of the Three ORC Approaches for Possible Working Fluids in This Paper

The maximum net power output values are calculated for all possible working fluids with all criteria proposed in this paper. The ranges of evaporative temperature and supercritical pressure for three ORC approaches analyses are shown in equations (24), (25) and (26).

The range of evaporative temperature for subcritical approach analysis is:

$$T_{evp} \in (T_{cond}, T_{tn}] \tag{24}$$

The range of evaporative temperature for superheated approach analysis is:

$$T_{evp} \in (T_{cond}, T_{crit} - 5] \tag{25}$$

The range of supercritical pressure for supercritical approach analysis is:

$$p_{scrit} \in [p_{cr} + 0.5, 10] \tag{26}$$

5.1 Results comparison

The optimum evaporative temperature or optimum supercritical pressure, optimum working fluid mass flow rate, net power output, ORC thermal efficiency, ORC exergy efficiency and specific net power output are calculated and presented in Table 7. Fig. 19, Fig 21 and Fig. 23 show the net power output and specific net power output for subcritical, superheated and subcritical respectively with the order of optimum net power for different working fluids from high to low. Similarly, Fig. 20 Fig. 22 and Fig. 24 present the ORC thermal efficiency and ORC exergy efficiency with working fluid net power output ranking from high to low.

The net power output, specific net power output, ORC thermal efficiency and exergy efficiency are the factors used to compare different working fluids. In Fig. 19 and Fig. 21, it is obvious that R218 has the noteworthy low net power output and specific net power output for subcritical ORC and superheated ORC due to its relatively low critical temperature as well as low critical pressure. The thermodynamic performance of working fluid for subcritical and superheated ORC is highly related to its critical temperature and pressure. R32 with the comparable low critical temperature as R218 generates 3.5320 MW_e which ranks third for superheated ORC approach. The reason is that R32 has the highest critical pressure among all working fluids listed in this paper. However, the specific net power output and efficiencies of R32 for superheated ORC are lower compared with the working fluids with similar net power output shown in Fig. 23. Therefore, the high net power output, specific net power output and cycle efficiencies will be achieved for working fluids with both high critical temperatures and pressures in subcritical ORC and superheated ORC cases. Besides R218, the net power output of other possible working fluids for subcritical ORC in the range of 3.2 MW_e to 4.2 MW_e and for superheated ORC in the range of 2.4 MW_e to 3.7 MW_e which are not fluctuating dramatically. However, the specific net power outputs vary significantly even the working fluids with similar net power outputs and cycle efficiencies. Meanwhile, the ORC thermal efficiency and exergy efficiency are not completely correlated with the net power output. For supercritical ORC approach, the wet working fluids have relatively higher net power outputs. However, the larger mass flow rates are needed for wet working fluids leading to the lower specific net power outputs. The net power output and efficiencies of supercritical ORC approach are larger than the subcritical ORC approach and superheated ORC approach.

Based on the analyses above, the selection decision of the working fluids cannot be made by only one or another factor. It is necessary to come up with a procedure to compare the working fluid thermodynamic performance comprehensively. In order to select the most suitable working fluids among the list for each ORC approach, the median values of net power output, specific net power output, thermal efficiency and exergy efficiency are considered that the working fluids would be selected when the net power output, specific net power output and cycle efficiencies equal to or are greater than the median values of all factors for the working fluids in Table 7. However, it can be seen from Fig. 19 to Fig. 24 that some values are very close to the median value although they are less than that. In some cases, all other factors meet the requirement but only one will be slightly less than the median value. Therefore, 5% of median value as the tolerance is added to pick out the suitable working fluids. The working fluid selection criteria are as follows:

a. Net power output equals to or is greater than 95% of the median value;
b. Specific net power output equals to or is greater than 95% of the median value;
c. Cycle efficiencies equals to or are greater than 95% of the median value;

The final selection results for all three approaches are listed below:

Subcritical: R236ea, R600a (flammable), R600 (flammable), R245fa, R365mfc, R601a (flammable), R601 (flammable), R123;

Superheated: R152a, R142b, R21, R600a (flammable), R141b, R236ea, R245fa, R600 (flammable);

Supercritical: R32, R22, R365mfc, R601 (flammable), R601a (flammable), R134a, R245fa, R600 (flammable), R152a, R600a, R142b.

The working fluids are listed in the order of high net power output to low net power output for each approach.

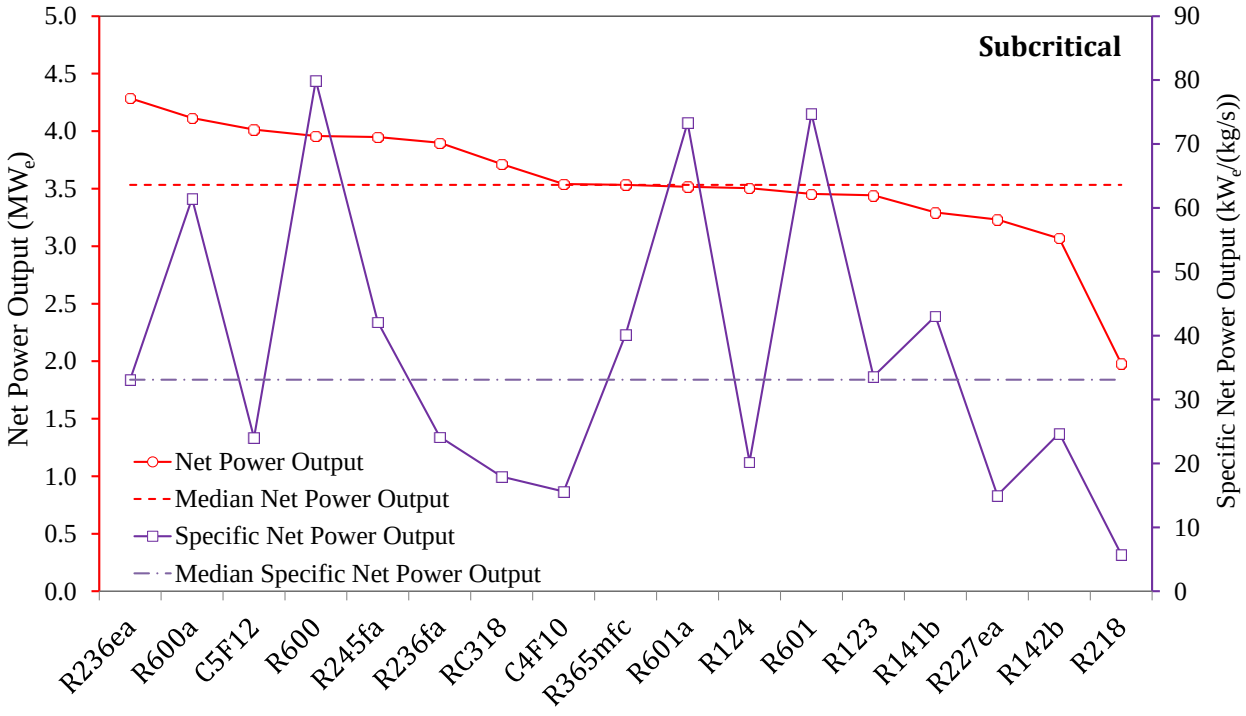

Fig. 19. Net Power Output and Specific Net Power Output of Subcritical Approach for All Possible Working Fluids

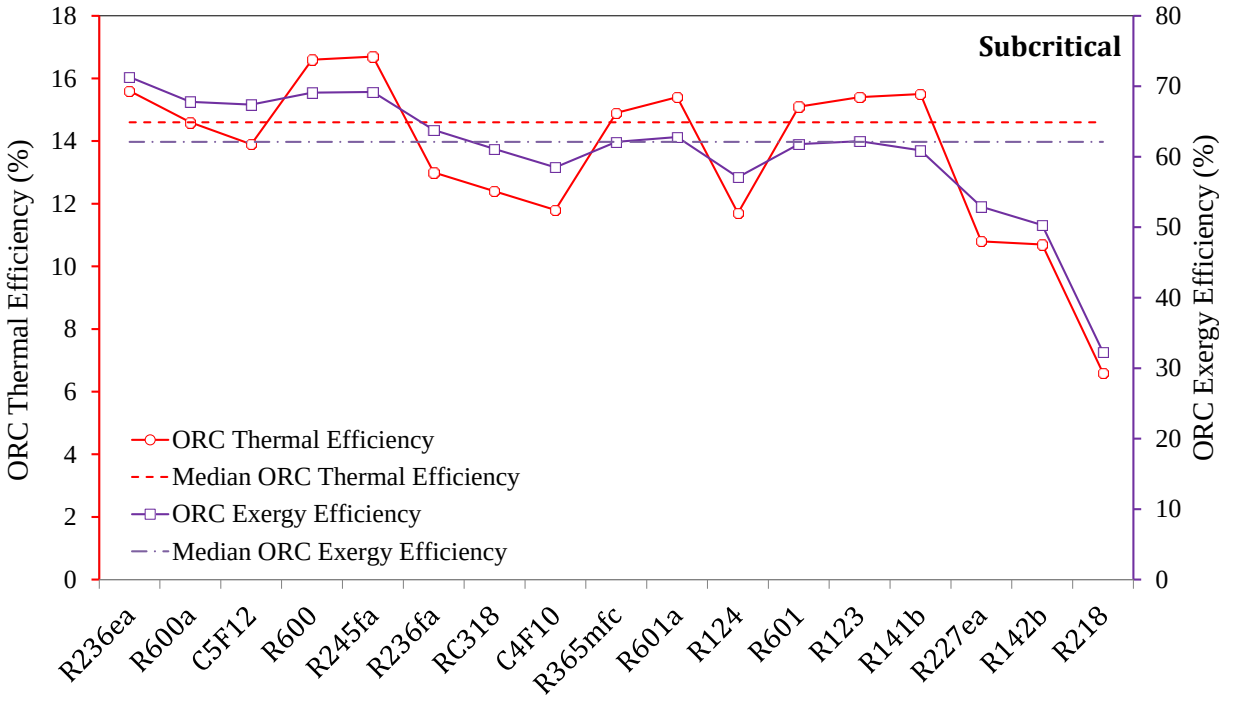

Fig. 20. ORC Thermal and Exergy Efficiency of Subcritical Approach for All Possible Working Fluids

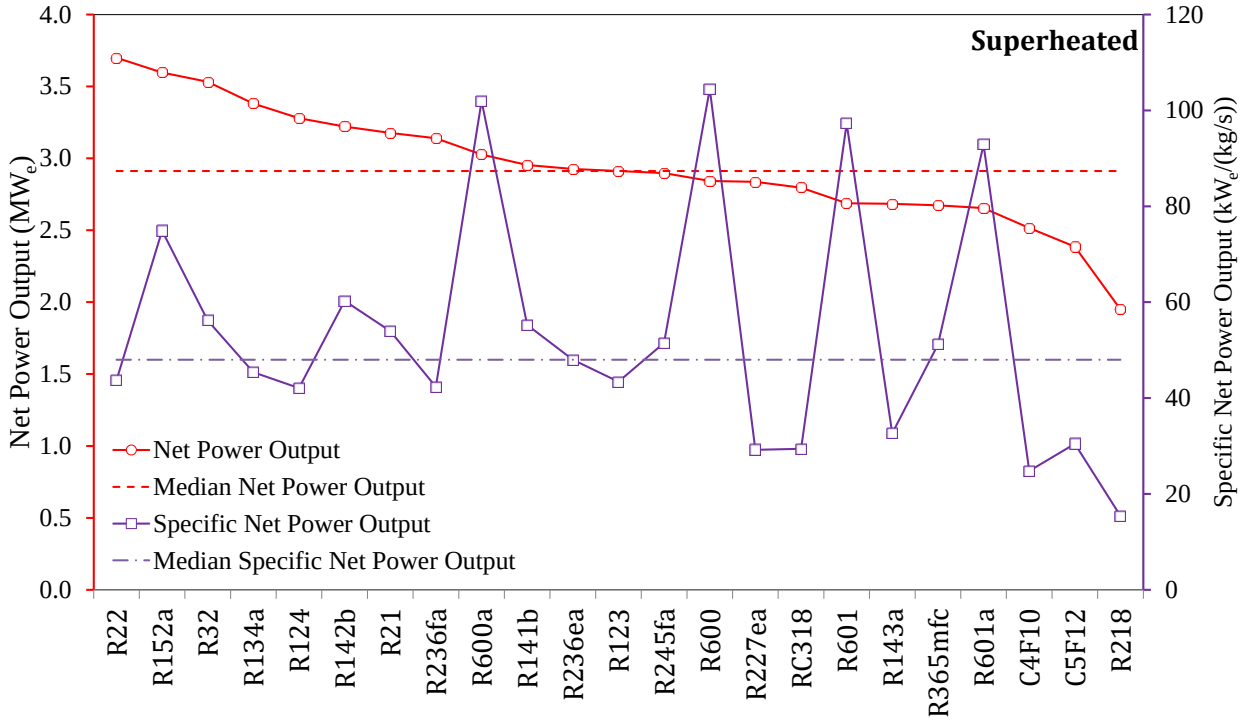

Fig. 21. Net Power Output and Specific Net Power Output of Superheated Approach for All Possible Working Fluids

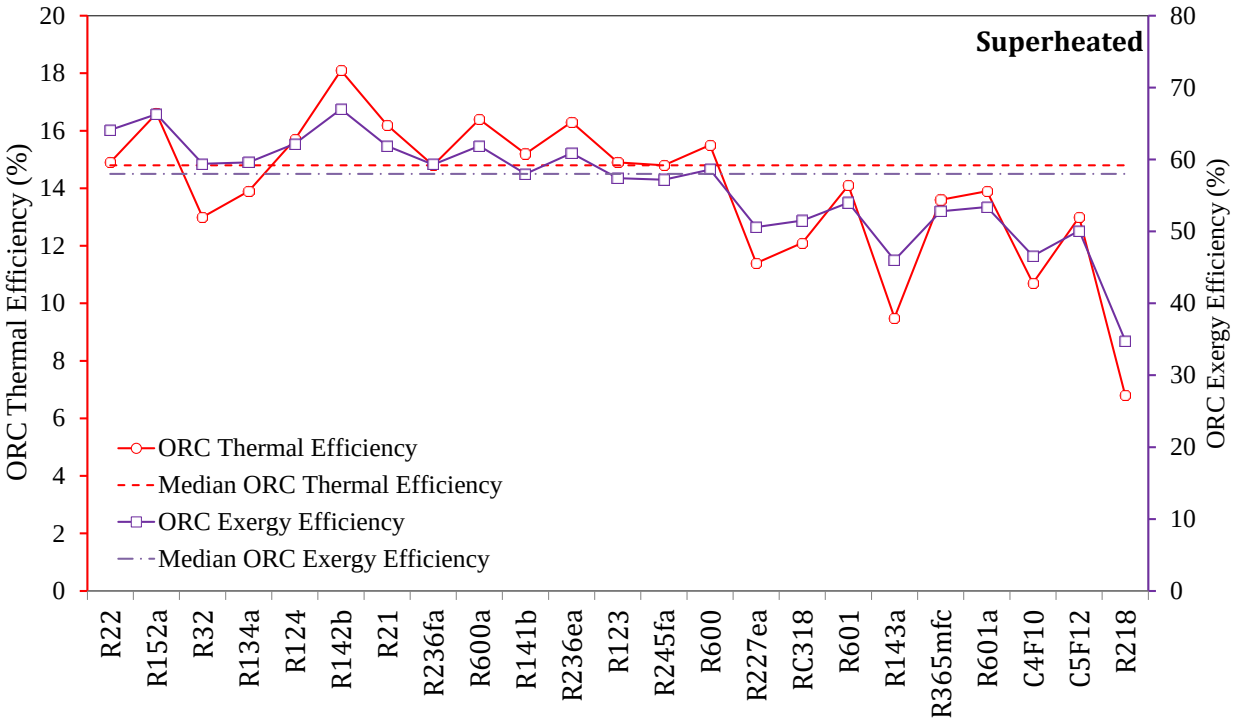

Fig. 22. ORC Thermal and Exergy Efficiency of Superheated Approach for All Possible Working Fluids

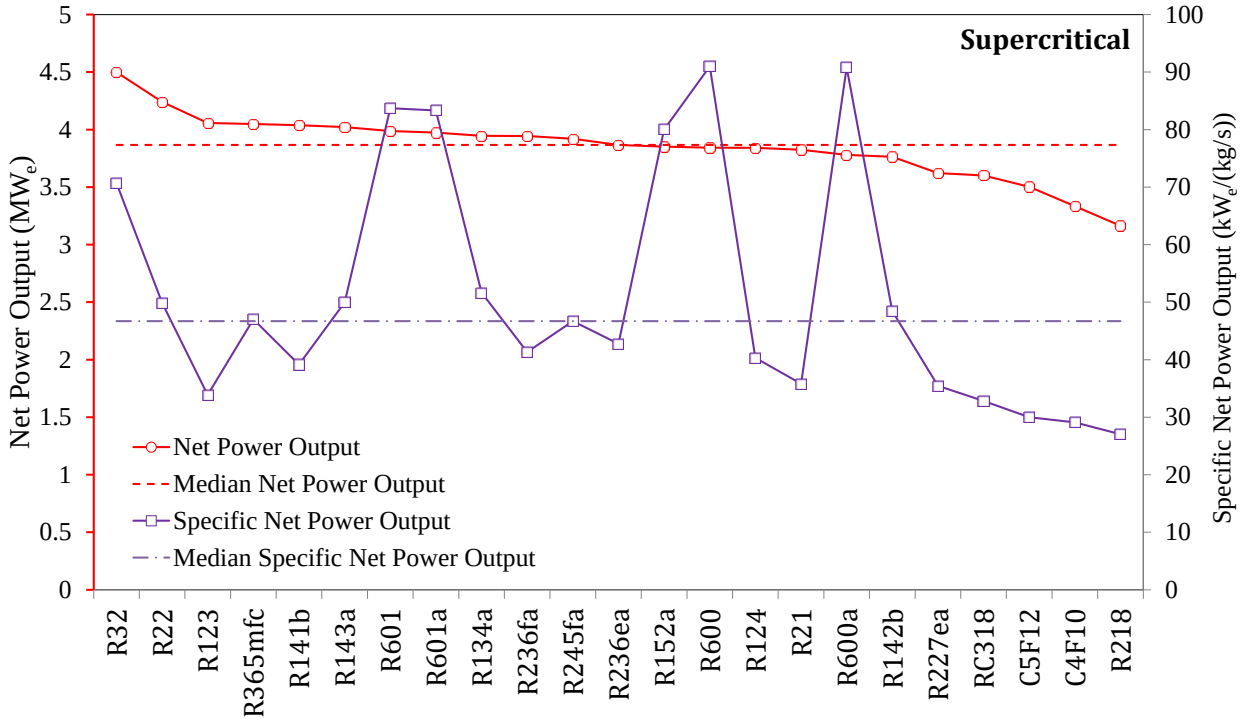

Fig. 23. Net Power Output and Specific Net Power Output of Supercritical Approach for All Possible Working Fluids

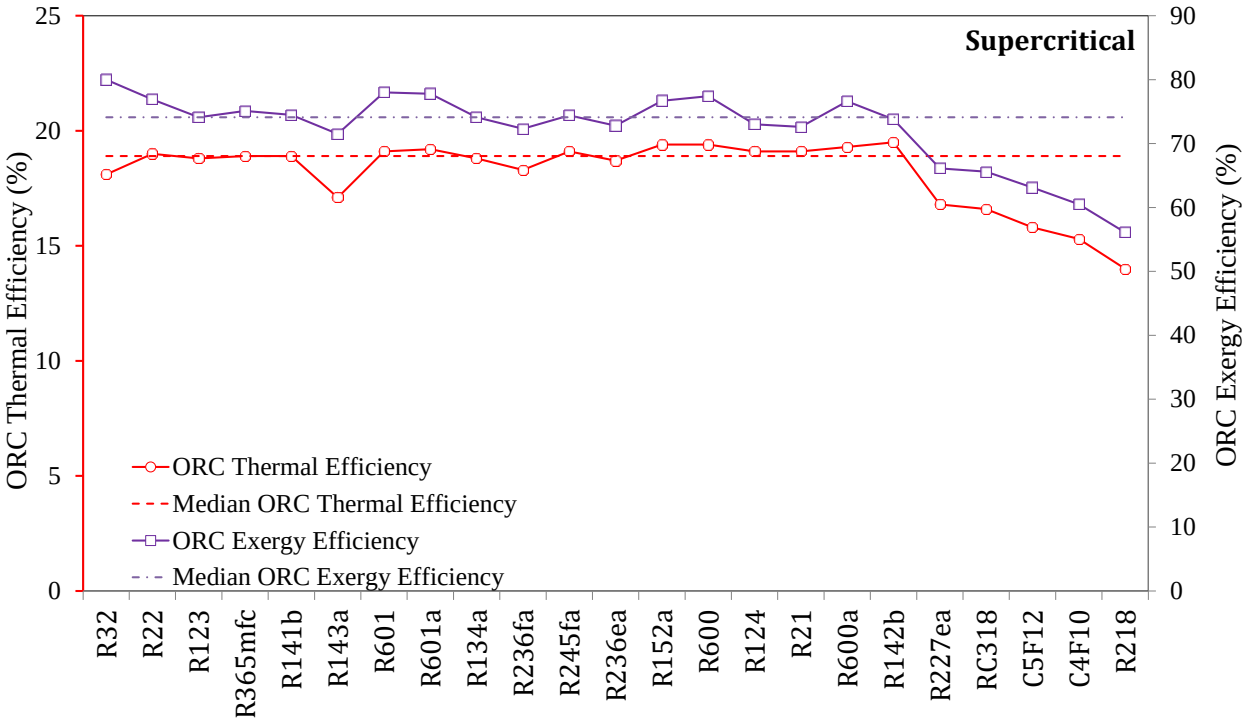

Fig. 24. ORC Thermal and Exergy Efficiency of Supercritical Approach for All Possible Working Fluids

Table 7

Optimum Simulation Results of Three Different ORC Approaches for Possible Working Fluids.

Working Fluid	Turning Point (℃)	Subcritical Approach						Superheated Approach						Supercritical Approach					
		$T_{evp,opt}$ (℃)	$\dot{m}_{WF,opt}$ (kg/s)	W_{net} (MW_e)	$\eta_{ORC,th}$ (%)	$\eta_{ORC,ex}$ (%)	w_{net} (kW_e/(kg/s))	$T_{evp,opt}$ (℃)	$\dot{m}_{WF,opt}$ (kg/s)	W_{net} (MW_e)	$\eta_{ORC,th}$ (%)	$\eta_{ORC,ex}$ (%)	w_{net} (kW_e/(kg/s))	$p_{evp,opt}$ (MPa)	$\dot{m}_{WF,opt}$ (kg/s)	W_{net} (MW_e)	$\eta_{ORC,th}$ (%)	$\eta_{ORC,ex}$ (%)	w_{net} (kW_e/(kg/s))
R123	150.62	106.68	102.40	3.4423	15.4	62.2	33.62	103.68	67.09	2.9118	14.9	57.4	43.40	10	119.80	4.0575	18.8	74.1	33.87
R124	82.93	82.93	173.14	3.5043	11.7	57.1	20.24	117.28	77.95	3.2797	15.7	62.2	42.07	10	95.29	3.8410	19.1	73.0	40.31
R134a	wet fluid	-	-	-	-	-	-	96.06	74.50	3.3810	13.9	59.6	45.38	10	76.40	3.9459	18.8	74.1	51.65
R141b	166.11	103.35	76.50	3.2931	15.5	60.9	43.05	100.35	53.46	2.9534	15.2	58.0	55.24	10	103.17	4.0383	18.9	74.5	39.14
R142b	73.99	73.99	124.16	3.0681	10.7	50.3	24.71	132.11	53.44	3.2213	18.1	67.0	60.28	10	77.68	3.7644	19.5	73.8	48.46
R143a	wet fluid	-	-	-	-	-	-	67.71	82.21	2.6836	9.5	46.0	32.64	10	80.46	4.0219	17.1	71.5	49.99
R152a	wet fluid	-	-	-	-	-	-	108.26	48.02	3.5974	16.6	66.3	74.91	6.997	48.14	3.8512	19.4	76.7	79.99
R21	wet fluid	-	-	-	-	-	-	99.33	58.88	3.1771	16.2	61.9	53.96	10	106.87	3.8256	19.1	72.6	35.80
R218	55.51	55.51	343.64	1.9789	6.6	32.3	5.76	66.87	126.51	1.9500	6.8	34.8	15.41	10	117.06	3.1649	14.0	56.1	27.04
R22	wet fluid	-	-	-	-	-	-	91.15	84.58	3.6991	14.9	64.1	43.73	8.740	85.02	4.2418	19.0	76.9	49.89
R227ea	82.56	82.56	215.37	3.2317	10.8	52.9	15.01	96.75	97.14	2.8366	11.4	50.6	29.20	10	102.15	3.6219	16.8	66.1	35.46
R236fa	97.47	97.47	161.32	3.8990	13.0	63.8	24.17	119.92	74.14	3.1397	14.8	59.3	42.35	10	95.40	3.9439	18.3	72.3	41.34
R236ea	122.93	122.93	129.48	4.2861	15.6	71.3	33.10	134.29	61.01	2.9263	16.3	60.9	47.97	10	90.43	3.8662	18.7	72.8	42.75
R245fa	127.02	127.02	93.68	3.9490	16.7	69.2	42.15	110.01	56.24	2.8973	14.8	57.2	51.51	10	83.92	3.9199	19.1	74.4	46.71
RC318	100.69	100.69	207.06	3.7135	12.4	61.1	17.93	110.23	95.10	2.7967	12.1	51.5	29.41	10	109.69	3.6016	16.6	65.6	32.83
R32	wet fluid	-	-	-	-	-	-	73.11	62.85	3.5320	13.0	59.4	56.20	10	63.66	4.4993	18.1	80.0	70.67
R365mfc	170.44	107.85	87.95	3.5337	14.9	62.1	40.18	105.85	52.24	2.6735	13.6	52.8	51.18	10	86.08	4.0487	18.9	75.1	47.04
C_4F_{10}	103.38	103.38	226.99	3.5405	11.8	58.5	15.60	108.18	101.53	2.5156	10.7	46.6	24.78	10	114.61	3.3344	15.3	60.5	29.09
C_5F_{12}	141.17	141.17	167.11	4.0132	13.9	67.4	24.02	142.41	78.34	2.3862	13.0	50.1	30.46	10	116.78	3.5029	15.8	63.1	29.99
R600	125.23	125.23	49.51	3.9578	16.6	69.1	79.95	116.98	27.20	2.8434	15.5	58.6	104.52	10	42.23	3.8429	19.4	77.4	91.00
R600a	107.79	107.79	66.92	4.1145	14.6	67.8	61.48	129.66	29.69	3.0270	16.4	61.9	101.95	10	41.62	3.7800	19.3	76.6	90.83
R601	179.40	106.55	46.21	3.4543	15.1	61.8	74.75	106.55	27.62	2.6880	14.1	54.0	97.31	10	47.63	3.9872	19.1	78.0	83.71
R601a	171.10	110.70	47.96	3.5166	15.4	62.8	73.33	107.20	28.57	2.6538	13.9	53.4	92.89	10	47.68	3.9735	19.2	77.8	83.33

5.2 Optimization Possibilities

In this paper, the simple ORC has been used for working fluid selection to simplify the analyses. There is still potential to improve the net power output and efficiencies of ORC beyond the simple ORC design. The regenerative ORC has gained attentions which has the ability to improve cycle efficiency. As shown in Fig. 25, heat is transferred from hot working fluid at turbine outlet to cold working fluid at evaporator inlet in recuperator. If the same amount of power is generated, less heat transfer surface area is needed for evaporator which leads to more economic design. In addition, thermal performance is improved due to less heat is rejected. Therefore, the working fluid selection analyses are worth being performed for the ORC using hot produced sCO_2 from geothermal reservoirs.

Other than the regenerative ORC, a coupled ORC system in Fig. 26 is proposed preliminarily by the author. Without obtaining the optimum organic working fluid flow rate for the maximum net power output, the smaller mass flow rate of working fluid 1 shown in Fig. 26 can be specified. Consequently, the sCO_2 temperature at the evaporator 1 outlet will be higher since less energy is transferred to the working fluid. Furthermore, directly reject the heat of high temperature sCO_2 will not be efficient. To add another bottom ORC power generation system which is called coupled ORC system is worth being investigated. It shows in Table 7 that some working fluids have evaporative temperature below 100 ℃ which are highly possible to be used as the bottom cycle working fluids. Nevertheless, the new objective function of total net power output and system thermal, exergy efficiency should be considered instead of the single simple cycle for working fluid selection.

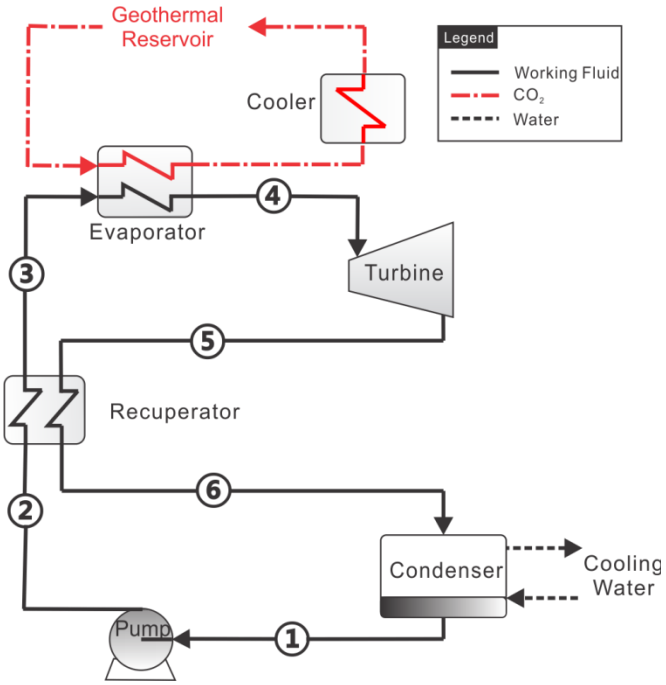

Fig. 25. Regenerative ORC

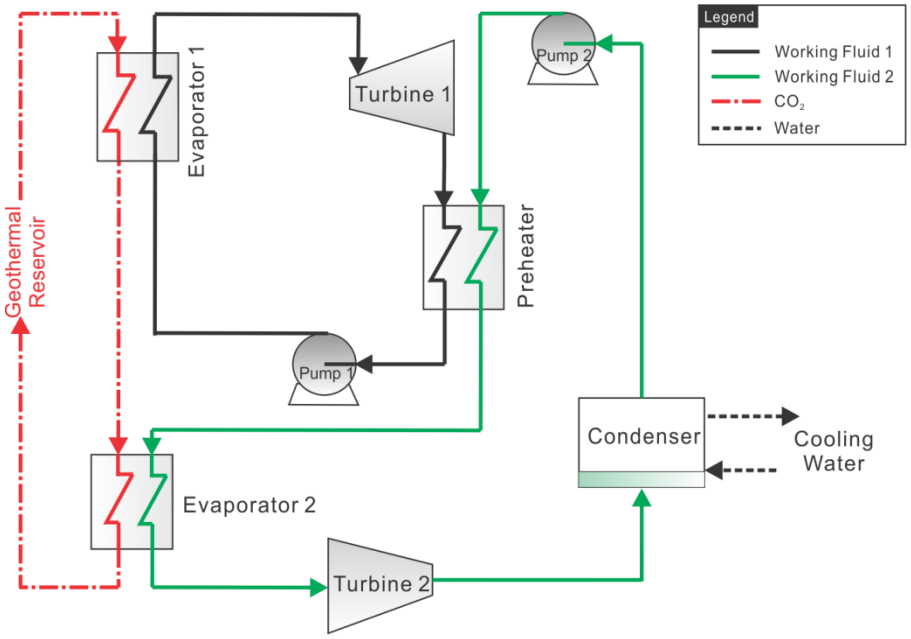

Fig. 26. Coupled ORC

6. Conclusion and Future Work

This study presents a procedure to select working fluid for subcritical, superheated and supercritical ORC approaches. The concepts of turning point for dry and isentropic working fluids and minimum turbine inlet temperature for wet working fluid have been introduced in this paper. Detailed pre-selection criteria for ORC working fluid have been proposed. A thermodynamic model with the capabilities to obtain optimum working fluid mass flow rate and evaluate thermal performance of the three ORC approaches has been developed. Based on the simulation results and analyses, the conclusions are derived as follows:

1) Net power output, specific net power output, ORC thermal efficiency and ORC exergy efficiency are the factors calculated for selecting suitable working fluids; the flammability, safety and environment impacts are also considered.
2) The thermodynamic performance of working fluid for subcritical and superheated ORC is highly related to its critical temperature and pressure. The high net power output, specific net power output and cycle efficiencies will be achieved at the same time with working fluid which has both high critical temperature and pressure;
3) The wet working fluids have relatively large net power output for supercritical ORC;
4) The suitable working fluids for each approach:
    - Subcritical: R236ea, R600a (flammable), R600 (flammable), R245fa, R365mfc, R601a (flammable), R601 (flammable), R123;
    - Superheated: R152a, R142b, R21, R600a (flammable), R141b, R236ea, R245fa, R600 (flammable);
    - Supercritical: R32, R22, R365mfc, R601 (flammable), R601a (flammable), R134a, R245fa, R600 (flammable), R152a, R600a, R142b.

In addition, the optimization options such as regenerative ORC and coupled ORC are discussed briefly. The improved working fluid selection procedures and thermodynamic performances need to be investigated as the follow-up work of this paper.

Apparently, the thermodynamic performance of ORC power generation system using hot produced sCO_2 is highly related to sCO_2 conditions produced from geothermal reservoirs, such as well distance, CO_2 injection flow rate, CO_2 injection temperature and reservoir conditions etc.

However, the hot produced sCO_2 conditions used in this paper are very typical and representative. Furthermore, the not significant changes in produced sCO_2 temperature and pressure would not affect the working fluid selection criteria discussed in the present paper.

The more detailed simulations and optimization study for geothermal heat mining using CO_2 have been performed which will be presented in a separate paper to obtain the optimum design and configuration of geothermal heat mining using CO_2. Furthermore, it is also not enough for engineering the practical ORC application only based on the thermodynamic performance. The cost analyses are very necessary to be performed to make the final infrastructure fabrication decision. Nevertheless, the cost study has to be based on the thermodynamic analyses which are presented in this paper.

Acknowledgements

This study was funded by the Mexican National Council of Science and Technology (CONACYT in Spanish), under the Sectorial Fund for Energy Sustainability, CONACYT-Secretary of Energy (No. S0019-2012-04). The team formed by the Lehigh University Energy Research Center and the University Michoacana de San Nicolás de Hidalgo, are grateful to the administrators of the Mexican Center for Innovation in Energy-Geothermal (CEMIE-Geo in Spanish) for their support and administration of the program. Additionally, thanks to the University of California, Berkeley, for providing the research version of the T2Well/ECO2N v.2 code for high temperature simulations and the valuable suggestions.

Reference

1. Leung, D.Y.C., G. Caramanna, and M.M. Maroto-Valer, *An overview of current status of carbon dioxide capture and storage technologies.* Renewable and Sustainable Energy Reviews, 2014. **39**: p. 426-443.
2. Brown, D.W., *Geothermal power production utilizing supercritical CO_2 combined with deep earth carbon sequestration.* Abstracts of Papers of the American Chemical Society, 2000. **220**: p. U399-U399.
3. Pruess, K., *Enhanced geothermal systems (EGS) using CO_2 as working fluid—A novel approach for generating renewable energy with simultaneous sequestration of carbon.* Geothermics, 2006. **35**(4): p. 351-367.

4. Pruess, K., *On production behavior of enhanced geothermal systems with CO2 as working fluid.* Energy Conversion and Management, 2008. **49**(6): p. 1446-1454.
5. Randolph, J.B. and M.O. Saar, *Coupling carbon dioxide sequestration with geothermal energy capture in naturally permeable, porous geologic formations: Implications for CO_2 sequestration.* Energy Procedia, 2011. **4**: p. 2206-2213.
6. Garapati, N., J.B. Randolph, and M.O. Saar, *Brine displacement by CO_2 , energy extraction rates, and lifespan of a CO 2 -limited CO 2 -Plume Geothermal (CPG) system with a horizontal production well.* Geothermics, 2015. **55**: p. 182-194.
7. Adams, B.M., et al., *A comparison of electric power output of CO_2 Plume Geothermal (CPG) and brine geothermal systems for varying reservoir conditions.* Applied Energy, 2015. **140**: p. 365-377.
8. Adams, B.M., et al., *On the importance of the thermosiphon effect in CPG (CO_2 plume geothermal) power systems.* Energy, 2014. **69**: p. 409-418.
9. Pan, L.H. and C.M. Oldenburg, *T2Well-An integrated wellbore-reservoir simulator.* Computers & Geosciences, 2014. **65**: p. 46-55.
10. Pan, L., et al., *Multiphase and Non-isothermal Model for Coupled Wellbore-Reservoir Flow of Carbon Dioxide and Variable Salinity Water.* 2011.
11. Pan, C.J., et al., *Heat mining assessment for geothermal reservoirs in Mexico using supercritical CO2 injection.* Energy, 2016. **102**: p. 148-160.
12. Tchanche, B.F., et al., *Low-grade heat conversion into power using organic Rankine cycles – A review of various applications.* Renewable and Sustainable Energy Reviews, 2011. **15**(8): p. 3963-3979.
13. Bao, J.J. and L. Zhao, *A review of working fluid and expander selections for organic Rankine cycle.* Renewable & Sustainable Energy Reviews, 2013. **24**: p. 325-342.
14. Drescher, U. and D. Brüggemann, *Fluid selection for the Organic Rankine Cycle (ORC) in biomass power and heat plants.* Applied Thermal Engineering, 2007. **27**(1): p. 223-228.
15. Wang, E.H., et al., *Study of working fluid selection of organic Rankine cycle (ORC) for engine waste heat recovery.* Energy, 2011. **36**(5): p. 3406-3418.
16. Rayegan, R. and Y.X. Tao, *A procedure to select working fluids for Solar Organic Rankine Cycles (ORCs).* Renewable Energy, 2011. **36**(2): p. 659-670.
17. Martinez-Gomez, J., et al., *A multi-objective optimization approach for the selection of working fluids of geothermal facilities: Economic, environmental and social aspects.* J Environ Manage, 2017.
18. Desai, N.B. and S. Bandyopadhyay, *Thermo-economic analysis and selection of working fluid for solar organic Rankine cycle.* Applied Thermal Engineering, 2016. **95**: p. 471-481.

19. Pan, L., et al., *Fully coupled wellbore-reservoir modeling of geothermal heat extraction using CO_2 as the working fluid.* Geothermics, 2015. **53**: p. 100-113.
20. Liu, B.T., K.H. Chien, and C.C. Wang, *Effect of working fluids on organic Rankine cycle for waste heat recovery.* Energy, 2004. **29**(8): p. 1207-1217.
21. Invernizzi, C., P. Iora, and P. Silva, *Bottoming micro-Rankine cycles for micro-gas turbines.* Applied Thermal Engineering, 2007. **27**(1): p. 100-110.